

Andrews University

Digital Commons @ Andrews University

Faculty Publications

4-2-2020

Optically Targeted Search for Gravitational Waves Emitted by Core-Collapse Supernovae During the First and Second Observing Runs ff Advanced LIGO and Advanced Virgo

Tiffany Summerscales
Andrews University, tzs@andrews.edu

LIGO Scientific Collaboration and the Virgo Collaboration

ASAS=SN Collaboration

DLT40 Collaboration

Follow this and additional works at: <https://digitalcommons.andrews.edu/pubs>



Part of the [Astrophysics and Astronomy Commons](#)

Recommended Citation

Summerscales, Tiffany; LIGO Scientific Collaboration and the Virgo Collaboration; ASAS=SN Collaboration; and DLT40 Collaboration, "Optically Targeted Search for Gravitational Waves Emitted by Core-Collapse Supernovae During the First and Second Observing Runs ff Advanced LIGO and Advanced Virgo" (2020). *Faculty Publications*. 1203.

<https://digitalcommons.andrews.edu/pubs/1203>

This Article is brought to you for free and open access by Digital Commons @ Andrews University. It has been accepted for inclusion in Faculty Publications by an authorized administrator of Digital Commons @ Andrews University. For more information, please contact repository@andrews.edu.

An Optically Targeted Search for Gravitational Waves emitted by Core-Collapse Supernovae during the First and Second Observing Runs of Advanced LIGO and Advanced Virgo

LIGO Scientific Collaboration, Virgo Collaboration, ASAS-SN Collaboration, DLT40 Collaboration, and F. Salemi
(Dated: 22 August 2019)

We present the results from a search for gravitational-wave transients associated with core-collapse supernovae observed within a source distance of approximately 20 Mpc during the first and second observing runs of Advanced LIGO and Advanced Virgo. No significant gravitational-wave candidate was detected. We report the detection efficiencies as a function of the distance for waveforms derived from multidimensional numerical simulations and phenomenological extreme emission models. For neutrino-driven explosions the distance at which we reach 50% detection efficiency is approaching 5 kpc, and for magnetorotationally-driven explosions is up to 54 kpc. However, waveforms for extreme emission models are detectable up to 28 Mpc. For the first time, the gravitational-wave data enabled us to exclude part of the parameter spaces of two extreme emission models with confidence up to 83%, limited by coincident data coverage. Besides, using *ad hoc* harmonic signals windowed with Gaussian envelopes we constrained the gravitational-wave energy emitted during core-collapse at the levels of $4.27 \times 10^{-4} M_{\odot} c^2$ and $1.28 \times 10^{-1} M_{\odot} c^2$ for emissions at 235 Hz and 1304 Hz respectively. These constraints are two orders of magnitude more stringent than previously derived in the corresponding analysis using initial LIGO, initial Virgo and GEO 600 data.

PACS numbers: 04.80.Nn, 07.05.Kf, 95.85.Sz, 97.60.Bw

I. INTRODUCTION

The direct detection in September 2015 of a binary black hole merger [1] initiated the field of gravitational-wave astronomy. During the first and second observing runs (O1 and O2) of Advanced LIGO and Advanced Virgo several more mergers were reported [2–7] and in August 2017 a binary neutron star merger [8] was observed in the gravitational-wave (GW) and electromagnetic spectra. This event gave birth to multimessenger astronomy with gravitational waves [9–13].

Core-collapse supernovae (CCSNe) are another important target of multimessenger astronomy with GWs, as all recorded supernovae were observed in the electromagnetic spectrum and low energy neutrinos were observed from SN 1987A [14–16]. GWs and neutrinos provide unique information about the dynamics of the collapse and the onset of the explosion, as opposed to electromagnetic emission which is delayed and originates in regions thousands of kilometers away from the central engine. Their observation could provide hints to the shock revival mechanism [17–23]. The most promising opportunity for multimessenger GW astronomy with CCSNe would be a Galactic CCSN, although the rate of such events is expected to be just one or two per century [24–30].

In contrast to all-sky, all-time unmodelled GW transient searches [31–34], targeted searches for CCSNe impose the sky location, the source distance, and a time window for the arrival time of the GW signal. In the previous CCSN targeted search with first-generation GW detector data [35] we developed the methodology, derived distance ranges for various GW emission processes, provided null model exclusion statements, and established GW energy constraints.

This paper describes a targeted search focusing on CC-

SNe recorded by astronomical observations at distances up to approximately 20 Mpc during O1 and O2. We selected five CCSNe, four of which are type-II supernovae (SN 2015as, SN 2016B, SN 2016X, SN 2017eaw) and one is type-Ib/c (SN 2017gax). We have not found any evidence for a GW signal associated with them. Similarly to [35], we obtain distance ranges for a selection of waveforms which were computed from numerical simulations and that are representative of different emission mechanisms and progenitors. We also use phenomenological waveforms representing possible but extreme emission models and we derive standard candle model exclusion statements for them. Finally, we adopt *ad hoc* sine-Gaussian waveforms to simulate GW emission in specific time-frequency regions allowing us to derive upper limits on the emitted GWs from a specific CCSN.

This paper is organized as follows: In Sec. II we list the CCSNe that we study in this search. We also describe

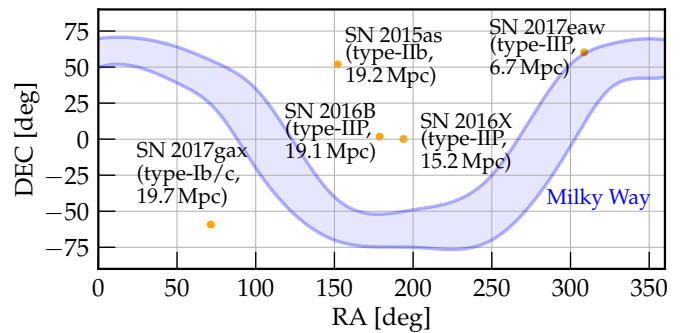


FIG. 1. Sky locations of core-collapse CCSNe analyzed in this search. All were recorded within 20 Mpc during the O1 and O2 observing runs.

TABLE I. Core-collapse supernovae selected as targets for the gravitational-wave search described in this paper. The variables t_1 and t_2 are the start and end of the on-source windows (OSWs), Δt is the duration of the OSWs, and OSW Method indicates how the OSW is calculated (see Sec. II A). The Run column indicates the LIGO and Virgo observing runs. The Active Detectors column lists the interferometers taking data during the on-source window. We include data from the LIGO Hanford (H1), LIGO Livingston (L1) and Virgo (V1) detectors. The last column presents coincident duty factors.

Supernova	Type	Host Galaxy	Distance [Mpc]	t_1 [UTC]	t_2 [UTC]	Δt [days]	OSW Method	Run	Active Detectors	Coincident Coverage
SN 2015as	I Ib	UGC 5460	19.2	2015 Nov 14.77	2015 Nov 16.23	1.47	Early	O1	H1,L1	34.2%
SN 2016B	I IP	PGC 037392	19.1	2015 Dec 23.51	2015 Dec 27.55	4.03	Early	O1	H1,L1	34.3%
SN 2016X	I IP	UGC 08041	15.2	2016 Jan 17.72	2016 Jan 20.56	2.86	Early	O1	H1,L1	14.4%
SN 2017eaw	I IP	NGC 6946	6.72	2017 Apr 26.56	2017 Apr 27.96	1.39	EPM	O2	H1,L1	48.8%
SN 2017gax	Ib/c	NGC 1672	19.7	2017 Aug 14.28	2017 Aug 16.15	1.66	Early	O2	H1,L1,V1	61.5% (H1L1) 60.8% (H1L1V1)

methods for calculating the time period when we expect the moment of collapse. In Sec. III we describe the data used in the search. Sec. IV describes the methodology, the pipeline, simulated GW signals, and systematic uncertainties. The results in Sec. V include distance reaches for several models of emission, GW energy constraints, and model exclusion statements. We draw conclusions in Sec. VI.

II. TARGETED CORE-COLLAPSE SUPERNOVAE

From all core-collapse supernovae recorded during the O1 and O2 periods, we have selected those that contribute to model exclusion statements and meet the following criteria: (i) the distance is less than approximately 20 Mpc, (ii) the period where we expect to find the GW transient, the on-source window, (see Sec. II A) is sufficiently well identified (order of days maximum), and (iii) there is sufficient GW detector data within the supernova on-source window to allow us to accumulate at least a few years of background data (see Sec. IV B).

During O1 and O2, astronomers found and followed-up numerous CCSNe in the nearby universe. Based on the information from Astronomical Telegrams [36] and supernova catalogs (ASAS-SN [37–40], DLT40 [41], Gaia [42, 43], ASRAS [44], TNS [45], OSC [46], CBAT [47]), we found 9 supernovae of interest.

Only five CCSNe meet the selection criteria and are used for the astrophysical statements in this paper. They are: SN 2015as, SN 2016B, SN 2016X, SN 2017eaw, and SN 2017gax. They are reported in Table I and Figure 1 presents their sky locations. The majority of these are type-II supernovae originating from red supergiant progenitor stars and the host galaxy was identified for each. The distance to each CCSNe is determined using the estimated distance to its host galaxy. The on-source window calculation methods are described Sec. II A.

SN 2015as, a type-I Ib supernova, was discovered on 2015 November 15.78 UTC [48] during O1. The host galaxy is UGC 5460 at a distance of 19.2 Mpc [49]. Although the spectrum transitions to a type-Ib supernova

around 75 days after explosion, the spectrum evolution closely relates to that of SN 2008ax, suggesting type-I Ib [49]. The progenitor star is either a main sequence $15 M_\odot$ star or $20 M_\odot$ Wolf-Rayet star [50]. CCSN ejecta is estimated to be $1.1 - 2.2 M_\odot$.

SN 2016B (ASASSN-16ab), a type-I IP supernova, was discovered by ASAS-SN on 2016 January 03.62 UTC [51] during O1. The host galaxy is PGC 037392 at a distance of 18.6 Mpc [51]. The progenitor star is estimated to be a red supergiant [52].

SN 2016X (ASASSN-16at), a type-I IP supernova, was discovered by ASAS-SN on 2016 January 20.59 UTC [53]. It exploded in the spiral galaxy UGC 08041 at a distance of 15.2 Mpc [54]. Optical observations in [54] indicate that the progenitor star is a massive red supergiant with an initial mass larger than $19 - 20 M_\odot$ and a radius larger than $930 \pm 70 R_\odot$.

SN 2017eaw (Gaia17bmy), a type-I IP supernova, was discovered by Gaia on 2017 May 14.24 UTC [55]. The CCSN exploded in galaxy NGC 6946, the estimated distance to be 6.72 ± 0.15 Mpc away [56]. This is the closest CCSN considered in the search. The analyses in [57–59] provide indication that the progenitor was a red supergiant with an estimated initial mass of $13 M_\odot$ and radius of $4000 R_\odot$.

SN 2017gax (DLT17ch), a type-Ib/c supernova, was discovered by the DLT40 on 2017 August 14.71 UTC [41]. This CCSN was found in NGC 1672, 19.7 Mpc away [60]. Unfortunately, little is known about the progenitor star.

Any CCSN, where the detection efficiencies for the extreme emission models are non-zero, and with sufficient on-source window coverage, helps the model exclusion probabilities (see Sec. V C). In this regard we also considered CCSNe at distances greater than 20 Mpc. Four other such CCSNe have been recorded during the O1 and O2 periods: not enough GW data was available for *SN 2016C* (type-I IP, 20.1 Mpc [61, 62]) and *SN 2017ein* (type-Ic, 11.2 Mpc [63, 64]), and no on-source window could be sufficiently constrained for *SN 2017aym* (Gaia17aks) (type-I IP, 26.4 Mpc [65, 66]) and *SN 2017bzb* (type-II, 13.9 Mpc [67, 68]). All the other CCSN candidates occurred outside the O1 and O2 periods or were located further than 20 Mpc.

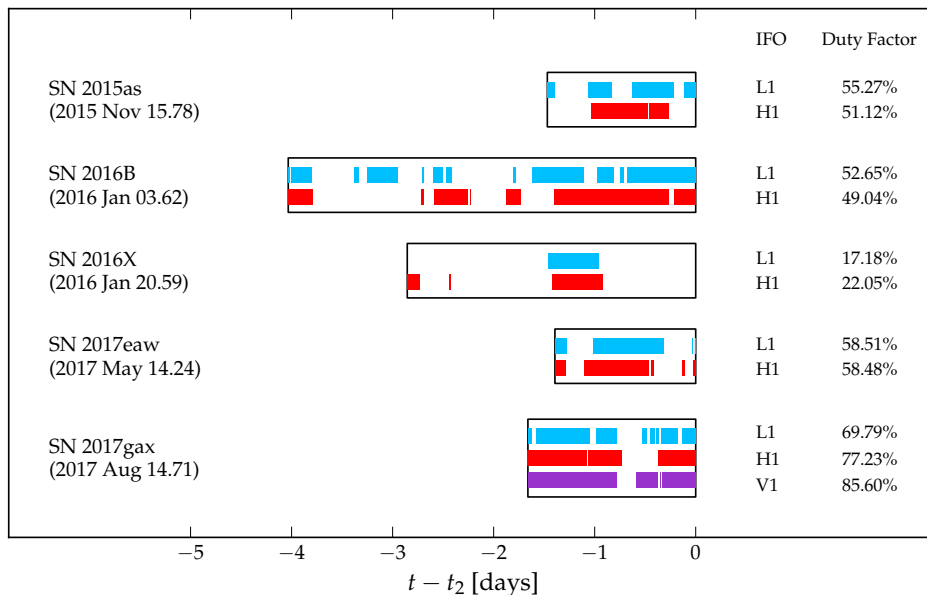


FIG. 2. Visual representation of the on-source windows (see Sec. II A), the data coverage for each detector, and the detector duty factors (percentage of available data inside on-source window). Dates in brackets are CCSN discovery times in UTC and t_2 is the end time of the on-source window for each CCSN. The plotted interferometers (IFO) are LIGO Hanford (H1), LIGO Livingston (L1) and Virgo (V1).

TABLE II. Overview of GW interferometers for the O1 and O2 observing runs from which we draw data for our search. The O1 observing run lasted four months and was followed by a half year maintenance period. The observing runs were preceded by engineering runs which we do not report here. O2 lasted around nine months, however the run was interrupted twice, between 2016.12.22–2017.01.04 and 2017.05.08–2017.06.26. The numbers in the table were calculated after periods of poor data quality were removed.

Run	Detectors	Run Period	Duty Factors	Coin. Duty Factor
O1	H1,L1	2015.09.12–2016.01.19	49.5% (H1), 42.4% (L1)	31.4% (H1L1)
O2	H1,L1	2016.11.30–2017.08.25	65.4% (H1), 63.6% (L1)	49.0% (H1L1)
O2	H1,L1,V1	2017.08.01–2017.08.25	77.7% (H1), 79.2% (L1), 85.1% (V1)	62.0% (H1L1V1)

A. On-source window calculation

The collapse of a star’s iron core forms a proto-neutron star and initiates a hydrodynamical shock wave propagating outward. Depending on the size of the progenitor star, the ensuing shock propagates for a period of seconds to days [69]. When it reaches the surface, i.e. shock breakout, a CCSN emits observable light. Because of weather conditions, limited sky coverage, and many other limitations, astronomical surveys typically record CCSNe hours to months after light first reaches Earth. The ability to extrapolate backwards in time to the moment of core-collapse, depends primarily on how quickly a CCSN is detected, its last non-detection, and the properties of its progenitor star.

The on-source window (OSW) is defined as the time interval $[t_1, t_2]$, where t_1 and t_2 are the beginning and end times respectively. An upper bound to this interval is t_{disc} , the time at which the CCSN was first observed electromagnetically. We define t_{Null} as the time of the last observation of a host galaxy without a supernova

present. To estimate the OSW we consider two methods. The choice between the *early observation method (Early)* and the *expanding photosphere method (EPM)* is based on the quality of the multi-band photometry, the determination of the host galaxy and the type of CCSN. We apply the early observation method when $t_{\text{disc}} - t_{\text{Null}}$ is of order a few days, the supernova type is known, and the progenitor star is inferred [70–73]. In all other cases, we consider the EPM.

In the early observation method, t_2 is the time when the CCSN is discovered, i.e. $t_2 = t_{\text{disc}}$. To determine t_1 , we need to take into account t_{Null} , and the shock propagation travel time between the moment of explosion and shock breakout, Δt_{SB} . We get that $t_1 = t_{\text{Null}} - \Delta t_{\text{SB}}$. Δt_{SB} depends mainly on the type of the progenitor star. Wolf-Rayet stars are stripped of helium and hydrogen and they lead to type-Ib/c supernovae. Their radii are on the order of a few R_{\odot} with typical shock breakout times ranging from a few seconds up to a minute [74]. Red supergiant stars have radii of 500-1000 R_{\odot} [75] and typical Δt_{SB} ranges from more than ten hours up to a

few days [76]. We calculated the OSW with the early observation method for four CCSNe: SN 2015as, SN 2016B, SN 2016X and SN 2017gax. For each of them we identified t_{Null} and t_{disc} based on the astronomical surveys. We calculated Δt_{SB} from information about their progenitor stars. To account for uncertainties in the progenitor star information, we enlarge the OSW by a number of hours (from 15 h up to 24 h [77, 78]).

The expanding photosphere method is used in astronomy primarily to estimate distances to CCSNe, but we employ it to estimate the time of core-collapse [79]. We briefly describe the method, but a detailed explanation can be found in [80–85]. When the shock breaks through a star’s surface, it heats up the outer layers and pushes them outwards. The expanding photosphere grows with time and its speed can be measured using Doppler shifts in its spectrum. As a consequence, we can extrapolate backward in time from the moment when explosion was caught in the optical bands in order to estimate t_1 and t_2 . Since the interval between $t_{\text{disc}} - t_{\text{Null}}$ for SN 2017eaw was greater than a week and because SN 2017eaw follow-up observations allow it [57, 58], we used the EPM to calculate the OSW.

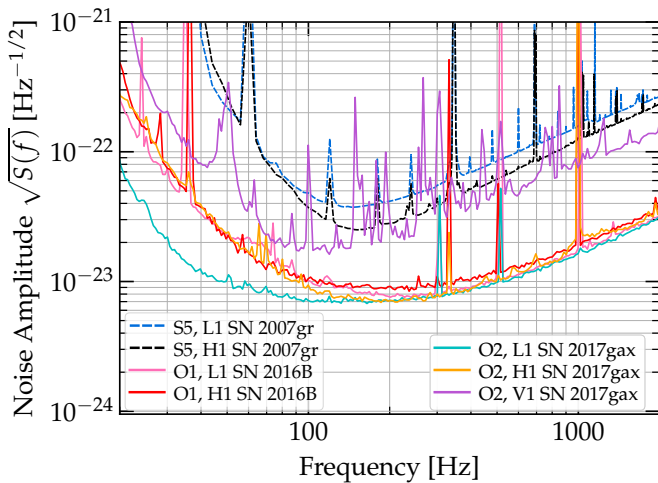


FIG. 3. Noise amplitude spectral densities of the GW interferometers. For SN 2016B and SN 2017gax we chose ten random periods inside the corresponding on-source windows. Each period was 10 minutes long. We calculated the noise spectra for each and then took an average. Amplitude spectra for SN 2007gr are reproduced from Ref. [35].

III. DETECTOR NETWORKS AND COVERAGE

Data from O1 and O2 were used for this search. This includes data from the Advanced LIGO detectors in Hanford (H1) and Livingston (L1) and the Advanced Virgo (V1) detector. O1 started on September 12, 2015 and ended on January 19, 2016, while O2 spanned the period between November 30, 2016 and August 25, 2017 [2]. The L1 and H1 detectors were observing jointly during

O1 and O2, and Virgo joined the LIGO detectors on August 1, 2017 [2].

The data are affected by instrumental and environmental sources of noise that prevent some of the data from being analyzed [86]. Periods of poor data quality are excluded using the information from many probes monitoring the environment of the detectors and probes controlling the different optical elements [87, 88]. For all CCSNe, we applied the same criteria for excluding times of poor data quality that were used in the all-sky short-duration unmodelled transient GW searches [33, 34].

Table II specifies the data taking periods along with the availability of each detector, which is referred to as the *duty factor*. The duty factor for each detector in O2 was higher than in O1 and was growing towards the end of the period. Figure 2 shows the OSWs for each CCSN together with the periods when detector data was available. The analysis is performed on data that is coincident between two or more detectors. OSW for SN 2016X extends past the end of O1.

Figure 3 shows the noise spectral density for all available detectors at the times of SN 2016B and SN 2017gax. For comparison, we plot the sensitivities of the two detectors for SN 2007gr [35] observed during LIGO Science Run 5 (S5). When comparing the data for SN 2007gr to the O1-O2 sensitivity, the detectors are 3 to 5 times more sensitive in the most sensitive detector band between 100 and 300 Hz [33] and around 10 times more sensitive around 1 kHz. Moreover, the low frequency part of the spectrum (below 100 Hz) improved during O2, especially in the L1 detector.

SN 2017gax happened in August 2017 when the LIGO and Virgo detectors were acquiring data. We have considered not only the H1L1 coincident time but also the H1L1V1 coincident time. Because of the sensitivity difference between Virgo and the two LIGO detectors, we found that the H1L1V1 network is less sensitive. We thus report results using the H1L1 network.

IV. METHODOLOGY

In this paper we search for GW signals in a large frequency band, 16-2048 Hz, without specific assumptions about the signal morphology. This frequency band allows us to cover most of the main emission processes inside a CCSN. We employ coherent WaveBurst (cWB) [96] as the search algorithm, which we describe in the following section.

A. Coherent Waveburst

Coherent WaveBurst is an excess power pipeline that is based on the constrained maximum likelihood ratio method [96]. For each event, the pipeline calculates correlation coefficients $cc = E_c / (E_c + E_n)$ which measures the degree of similarity of the waveforms between

TABLE III. Waveforms from detailed multidimensional CCSN simulations described in the text. For each waveform, we give the emission type, reference, waveform identifier, angle-averaged root-sum-squared strain h_{rss} , the frequency f_{peak} at which the GW energy spectrum peaks, the emitted GW energy E_{GW} , and available polarizations. See Refs. [89, 90] for details.

Waveform Family	Waveform Identifier	h_{rss} [$10^{-22}\sqrt{\text{s}} @ 10 \text{ kpc}$]	f_{peak} [Hz]	E_{GW} [$10^{-9}M_{\odot}c^2$]	Polarizations
Müller [91] 3D Convection and SASI	mul1-L15-3	1.655	150	3.741×10^{-2}	+, ×
	mul2-N20-2	3.852	176	4.370×10^{-2}	+, ×
	mul3-W15-4	1.093	204	3.247×10^{-2}	+, ×
Ott [92] 3D Convection and SASI	ott1-s27fheat1p05	0.238	1019	7.342×10^{-1}	+, ×
Yakunin [93] 2D Convection and SASI	yak1-B12-WH07	3.092	760	3.411	+
	yak2-B15-WH07	14.16	932	7.966	+
	yak3-B20-WH07	3.244	638	4.185	+
	yak4-B25-WH07	18.05	1030	14.21	+
Scheidegger [94] Rotating Core-Collapse	sch1-R1E1CA _L	0.129	1155	1.509×10^{-1}	+, ×
	sch2-R3E1AC _L	5.144	466	2.249×10^2	+, ×
	sch3-R4E1FC _L	5.796	698	4.023×10^2	+, ×
Dimmelmeier [95] Rotating Core-Collapse	dim1-s15A2O05ls	1.052	770	7.685	+
	dim2-s15A2O09ls	1.803	754	27.880	+
	dim3-s15A3O15ls	2.690	237	1.380	+

the detectors. E_c is the normalized coherent energy obtained by cross-correlating the reconstructed waveforms in each detector and E_n is the normalized per detector residual noise energy after the reconstructed waveform is subtracted from the data. For a real GW, $cc \approx 1$, and we accept events that have $cc > 0.8$. Each event is ranked according to a coherent network signal-to-noise ratio, $\rho \propto \sqrt{E_c}$. A more detailed explanation of these statistics is given in Refs. [87, 96].

The events are divided into two mutually exclusive classes based on their morphologies, similarly to [33]. Class *C1* contains transients of a few cycles. This class is primarily polluted by *blip* glitches which are very short duration transients, $O(10)$ ms, with large bandwidth, $O(100)$ Hz [86, 97]. These noise transients are currently of unknown origin. To separate blip glitches from the bulk of the trigger population in class *C2* we use the selection criteria described in [87].

B. Background estimation

As mentioned earlier, each GW detector is constantly monitored with various sensors that allow us to exclude poor data quality periods from the analysis. However, it is not possible to remove all sources of noise. To estimate how often the pipeline produces events that are falsely identified as GWs, we perform a background analysis where CWB artificially shifts the data in one detector with respect to the other. The typical time shift is a multiple of one second, which is much longer than the GW travel time between different detectors (e.g., 10 ms between H1 and L1). This allows us to estimate the false alarm rate (FAR) of the background events. We use a few years of background data for each CCSN.

GW events obtained when no shift is applied to the data may contain genuine GW signals. The events from

the search classes are combined and ranked with their FAR. We assume that the event with the smallest FAR between the two search classes is a potential GW candidate and we refer to it as the *loudest event*. The FAR is calculated from the noise transient distribution of the class to which the loudest event belongs. Since the classes are independent, we apply a trial factor 2 to the FAR (see also [1, 33]) of the loudest event. The significance of an event with given FAR is assessed by calculating its False Alarm Probability (FAP), which is the probability of obtaining one or more noise events that are less than or equally ranked:

$$\text{FAP} = 1 - \exp(-T_{\text{coinc}} \times \text{FAR}) \quad (1)$$

where T_{coinc} is the coincident data duration of the appropriate OSW.

C. Search sensitivity

We determine how sensitive the pipeline is to particular waveform families. CWB adds (*injects*) supernova waveforms to the detector data inside the OSW with the right time delay in each detector such that the GW signal comes from the accurately known CCSN sky location. The fraction of the injected signals that can be detected and pass the selection criteria is the *detection efficiency*. The injection procedure is repeated with waveform amplitudes corresponding to different source distances. We select any event that passes the selection criteria of the search and whose rank is smaller than the loudest event FAR.

We consider two sets of multidimensional supernova explosion models, extreme emission models, and *ad hoc* waveforms as listed in Tables III and IV. For all of the waveforms we provide the peak frequency, number of polarizations, and other quantities. For the waveforms from

multidimensional CCSN simulations and extreme emission models, we provide the GW energy, E_{GW} , emitted during the explosion and the source angle-averaged root-sum-squared GW strain,

$$h_{\text{rss}} = \sqrt{\int \langle h_+^2(t) + h_\times^2(t) \rangle_\Omega dt}. \quad (2)$$

Our efficiency estimates are subject to a number of uncertainties. The most important of these are calibration uncertainties in the strain data recorded at each detector, and Poisson uncertainties due to the use of a finite number of injections (Monte Carlo uncertainties). We use the same methodology explained in [35], to account for each of these uncertainties. For detection efficiencies, the dominant effect comes from the uncertainties in the strain amplitude calibration, as in [35]. These vary from a few percent at lower frequencies to 10% at higher frequencies in both L1 and H1. For this paper, these uncertainties are conservatively set to 10% for H1 and L1 at the times of the five CCSNe studied [98, 99]. The error analysis leads to decreasing the detection efficiencies by 9.1%.

For the waveforms coming from 2D simulations, marginalizing over all unknown angles the waveform amplitude is reduced by a factor $\sqrt{5/18}$ that we apply to the efficiencies. For optimally oriented CCSNe, the distance ranges for these models will be $\sqrt{18/5}$ times larger.

1. Waveforms from multidimensional CCSN simulations

The main mechanism behind a CCSN explosion is not yet fully understood and a complete review of the current state can be found in [21, 102–104] and in references therein. We divide the waveforms from multidimensional CCSN simulations into two sets according to their explosion mechanisms. In the first set, we consider a *neutrino-driven* explosion mechanism for non- or slowly-rotating progenitor stars. We employ three waveform families: Müller [91], Ott [92] and Yakunin [93]. In this scenario, neutrino heating plays a crucial role in creating the explosion. During the prompt convection, in the initial stages post bounce, GWs are emitted in the frequency range from 100-300 Hz, while at later times, GWs up to around 2 kHz can be expected [105, 106]. A typical duration for a GW transient is 0.5-1 s [21, 107, 108]. The second set of waveforms, with simulations from the Scheidegger [94] and Dimmelmeier [95] groups, utilizes the *magnetohydrodynamically-driven (MHD-driven)* explosion mechanism for rapidly rotating progenitor stars. The magnetic effects related to the rapid rotation may play a dominant role in creating the MHD-driven explosions. Note, however, almost all (99%) [21, 109] of explosions are believed to come from slowly rotating progenitor stars.

Müller *et al* [91] performed 3D simulations with a zero age main sequence (ZAMS) progenitor star of mass

$15 M_\odot$ (L15-3 and W15-4), and a $20 M_\odot$ (N20-2), which we refer to as *mul1*, *mul2* and *mul3* respectively. The simulations are three-dimensional and thus result in two polarizations. The convective movement of infalling matter and its interaction with the outer layers of the proto-neutron star result in GW emission in the frequency range 100-500 Hz.

Ott *et al* [92] produced a 3D simulation with a $27 M_\odot$ ZAMS progenitor star (*ott1*). The explosion becomes aspherical due to strong convection while the SASI visibility is weak. This model is rotating and a strong burst of GWs appears at the beginning of the explosion.

Yakunin *et al* [93] delivers waveforms from four 2D simulations (providing only one polarization state) corresponding to $12 M_\odot$, $15 M_\odot$, $20 M_\odot$, $25 M_\odot$ ZAMS progenitor stars. We denote them as *yak1*, *yak2*, *yak3* and *yak4* respectively. These waveforms capture several stages of the explosion. They show both low (SASI/convection) and high (g-mode) frequency components in their signals. Due to axisymmetry, the strain grows artificially over time, resulting in higher GW amplitudes than the 3D neutrino driven models.

Scheidegger *et al* [94] considers effects on the GW signature due to the equation of state, the initial rotation rate, and the magnetic fields. From an extensive set of waveforms, we extract three models, R1E1CA_L, R3E1AC_L, and R4E1FC_L, which we refer to as *sch1*, *sch2*, and *sch3*, respectively. All of these models are derived from the explosion of a $15 M_\odot$ ZAMS progenitor star. The models are three dimensional and produce two GW polarization states. The degree of rotation varies between the models; model R1E1CA_L has no rotation, which results in much lower GW energy in comparison to the rotating R3E1AC_L and R4E1FC_L models.

Dimmelmeier *et al* [95] performed 2D simulations (providing linearly polarized waveforms) with a $15 M_\odot$ ZAMS progenitor star. The waveforms contain very strong GW emission at the initial core-collapse and bounce that lasts less than 20 ms. We employ three waveforms with various degrees of rotation from moderate to rapid (*dim1-dim3*).

2. Extreme emission models

Along with the more realistic simulated CCSN explosions, we also consider two extreme scenarios: the *Long-Lasting Bar Mode* [100], and the *Torus Fragmentation Instability* [101]. The same models were used in [35], because even if they are unlikely to occur, they are not excluded [110].

In the first scenario, a very rapidly rotating progenitor star induces a bar mode instability in the proto-neutron star [94, 111–116]. This leads to large amplitude GWs that depend on the properties of the deformed proto-neutron star. We use the simple phenomenological bar model described in [100]. In this model, we use the following parameterization: the mass involved in the long-lasting bar mode of the proto-neutron star $M =$

TABLE IV. Waveforms from phenomenological and *ad hoc* emission models described in the text. For each waveform, we give the emission type, journal reference, waveform identifier, angle-averaged root-sum-squared strain h_{rss} , the frequency f_{peak} at which the GW energy spectrum peaks, the emitted GW energy E_{GW} , and available polarizations. See [89, 90] for details. As sine-Gaussian waveforms are *ad hoc*, they can be rescaled arbitrarily and do not have a defined physical distance or E_{GW} value.

Emission Type	Waveform Identifier	h_{rss} [$10^{-22} \sqrt{\text{s}} @ 10 \text{ kpc}$]	f_{peak} [Hz]	E_{GW} [$M_{\odot} c^2$]	Polarizations
Long-lasting Bar Mode [100]	lb1-M0.2L60R10f400t100	1.480	800	2.984×10^{-4}	+, ×
	lb2-M0.2L60R10f400t1000	4.682	800	2.979×10^{-3}	+, ×
	lb3-M0.2L60R10f800t100	5.920	1600	1.902×10^{-2}	+, ×
	lb4-M1.0L60R10f400t100	7.398	800	7.459×10^{-3}	+, ×
	lb5-M1.0L60R10f400t1000	23.411	800	7.448×10^{-2}	+, ×
	lb6-M1.0L60R10f800t25	14.777	1601	1.184×10^{-1}	+, ×
Torus Fragmentation Instability [101]	piro1-M5.0 η 0.3	2.550	2035	6.773×10^{-4}	+, ×
	piro2-M5.0 η 0.6	9.936	1987	1.027×10^{-2}	+, ×
	piro3-M10.0 η 0.3	7.208	2033	4.988×10^{-3}	+, ×
	piro4-M10.0 η 0.6	28.084	2041	7.450×10^{-2}	+, ×
sine-Gaussian [31]	sg1-235HzQ8d9linear	—	235	—	+
	sg2-1304HzQ8d9linear	—	1304	—	+
	sg3-235HzQ8d9elliptical	—	235	—	+, ×
	sg4-1304HzQ8d9elliptical	—	1304	—	+, ×

$\{0.2, 1.0\} M_{\odot}$, the radius $R = 10 \text{ km}$ and length $L = 60 \text{ km}$ of the bar, the spin frequency $f = \{400, 800\} \text{ Hz}$ along the direction perpendicular to the bar, and the duration $t = \{25, 100, 1000\} \text{ ms}$ of the deformation. We consider six waveforms, denoted as lb1-lb6, see Table IV for more details. Since the waveform amplitude is proportional to $M(L^2 - 3R^2)$ (see [100]), any combination of M , L and R giving the same value for $M(L^2 - 3R^2)$ as the six waveforms, will produce waveforms identical to the lb1-lb6 waveforms. Therefore results for lb1-lb6 waveforms are a good representation of the broader sections of parameter space.

In the second scenario, Piro and Pfahl [101] propose that, if a black hole and an accretion disk are formed during the collapse, the disk could fragment and large self-gravitating clumps of matter falling into the black hole would produce large amplitude GWs under the appropriate conditions. To model this signal we employ a simplified model [117] that depends on the mass of the central black hole $M_{\text{BH}} = \{5, 10\} M_{\odot}$ and the properties of the disk, namely the thickness of the torus $\eta = \{0.3, 0.6\}$ and the alpha viscosity parameter $\alpha = 0.1$. The torus thickness is defined as $\eta = H/r$, where H is the disk scale-height and r the local radius. For the disk model considered in [101], the mass of the fragmented clump is $M_f = 0.53\eta^3 M_{\text{BH}}$. The GW amplitude is proportional to the reduced mass of the BH-clump system, $\mu = M_{\text{BH}} M_f / (M_{\text{BH}} + M_f)$, which for the parameter space considered here ($M_f \ll M_{\text{BH}}$) is $\mu \approx M_f$.

3. Ad-hoc waveforms

We employ *ad hoc* waveforms to estimate the search sensitivity to short duration monochromatic signals that model GW emission in different frequency bands. We

use sine-Gaussian signals with a fixed central frequency $f_0 = \{235, 1304\} \text{ Hz}$ and duration $\tau = Q/(\sqrt{2\pi}f_0)$ where $Q = 8.9$ is the quality factor. In our analysis, we use four *ad hoc* waveforms denoted as sg1-sg4 that are linearly and elliptically polarized, see Table IV.

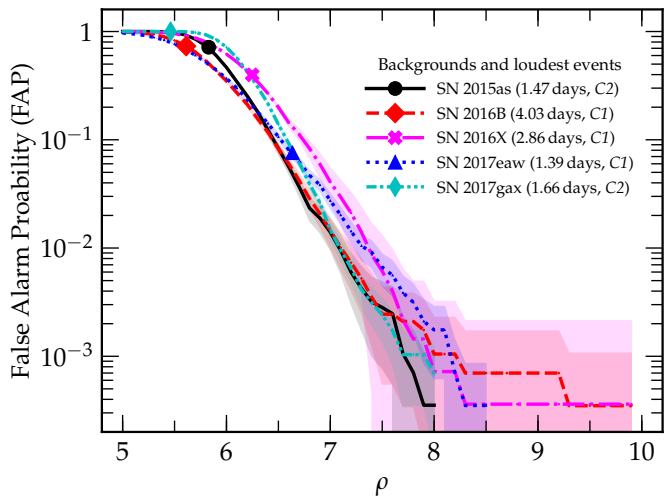


FIG. 4. The False Alarm Probability (FAP) of background events together with the loudest events for each CCSN. The non-negligible values of the FAP indicate that all the loudest events appear compatible with the noise background. The shaded region is the 1σ error. The numbers in the parentheses are durations of the on-source windows and the class where the loudest events belong.

V. SEARCH RESULTS

Figure 4 presents the background as a function of ρ the coherent network signal-to-noise ratio for all CCSNe. We

TABLE V. List of the loudest events for each CCSN. False alarm rate (FAR) and False Alarm Probability (FAP) for each of them indicate that they are consistent with background noise.

Supernova	Class	ρ	FAR [Hz]	FAP
SN 2015as	<i>C2</i>	5.8	2.9×10^{-5}	0.716
SN 2016B	<i>C1</i>	5.6	1.1×10^{-5}	0.732
SN 2016X	<i>C1</i>	6.2	1.4×10^{-5}	0.398
SN 2017eaw	<i>C1</i>	6.6	1.3×10^{-6}	0.076
SN 2017gax	<i>C2</i>	5.5	9.7×10^{-5}	1.000

plot the loudest events found in the OSWs with further detailed information given in Table V. The non-negligible values of the false alarm probabilities indicate that all the results appear compatible with the noise background. For each CCSN source, we estimate the search efficiency using the waveforms described in Sec. IV C considering events with a rank value smaller than the loudest event FAR.

A. Detection efficiency vs. distance

We provide detection efficiencies for waveforms listed in Table III and Table IV. Figure 5 presents the detection efficiencies for SN 2017eaw, the closest CCSN in this search. For reference, the plots show the distances to the Galactic center (8.5 kpc), the Large Magellanic Cloud (49.6 kpc [118]) that hosted SN 1987A, and the distance to the host galaxy of SN 2017eaw, NGC 6946. For each model, we determine the distance corresponding to a 50% detection efficiency. Distance reaches for each CCSN for neutrino-driven explosions and MHD-driven explosions are summarized in Table VI and extreme emission models in Table VII. For each model the distances are consistent across CCSNe and these distances are around 3-5 times further than in [35]. The largest distances are obtained for SN 2017gax. This can be explained by the fact that the loudest event for this CCSN has the lowest ρ value and the network sensitivity at the time of the CCSN was better over the duration of the OSW.

For the neutrino-driven explosions summarized in Table VI and the upper left panel of Figure 5, the detection distance reached less than 5 kpc. None of these models reach the Galactic center, however a few of the waveforms have non-zero detection probabilities at that distance. The least detectable models are the Müller waveforms because they are the least energetic. The most detectable models are the Yakunin waveforms and the reach increases with progenitor mass. The Ott model has a smaller detection reach compared to the Yakunin waveforms, but also has higher detection efficiency at small distances.

Table VI and the upper right panel of Figure 5 also present a summary of distance reaches for MHD-driven explosions. The distance reaches for most of these models are an order of magnitude larger than for the neutrino-

driven explosions. Some MHD-driven explosion models reach to the distance of Large Magellanic Cloud. If a MHD-driven supernova were to explode at the distance of SN 1987A, around 50 kpc away, we have a non-zero chance of detecting it. The detectable range for sch1 is two orders of magnitude shorter compared to those of sch2 and sch3. This Scheidegger model has a lower amplitude due to its slower rotation.

Distance reaches for the extreme emission models are given in Table VII and depicted in the bottom left panel of Figure 5. The ranges are on the order of several Mpc up to nearly 28 Mpc for the most extreme model. The reaches of a few waveforms exceed the distance of SN 2017eaw. Given the null detections, this means we can begin to exclude these models as discussed in Sec. V C.

The detection efficiencies for the linearly polarized waveforms (Dimmelmeier and Yakunin) do not reach unity even at small distances because the network of detectors is not sensitive to both polarizations for any sky position at a given time. There are sky positions where the detectors are insensitive to one of the polarizations and even a large amplitude signal with only one polarization will not be detectable. Waveforms with two polarizations are more efficiently detected than linearly polarized signals.

B. Constraints on GW energy emission

Similarly to [35] we provide constraints on the GW energy emission from CCSNe. This is the minimum energy emitted in GWs needed to be detectable with 50% probability. We calculate these constraints individually for each CCSN. We probe low- and high-frequency GW emission using sine-Gaussian *ad hoc* waveforms with central frequencies of 235 Hz and 1304 Hz (see Table IV). These waveforms do not have physical meaning, so we plot detection efficiency as a function of h_{rSS} (eqn. (2)) instead of distance. We assume isotropic emission with a total energy of

$$E_{\text{GW}} = \frac{\pi^2 c^3}{G} D^2 f_0^2 h_{\text{rSS}}^2, \quad (3)$$

where f_0 is the peak GW frequency of the sine-Gaussian, and D is the distance to the source [119].

The bottom right panel of Figure 5 shows the detection efficiency versus h_{rSS} for the four *ad hoc* waveforms. The quoted h_{rSS} for each sine-Gaussian corresponds to the strain with a 50% detection efficiency. The best sensitivity is achieved for the sine-Gaussians around 235 Hz (sg1 and sg3), which is a result of the lower noise level of the detectors at this frequency. The efficiency curves of the elliptically polarized waveforms (sg3 and sg4) flatten at higher detection efficiencies compared to the efficiencies for linearly polarized waveforms (sg1 and sg2) for the reason discussed in Sec. V A.

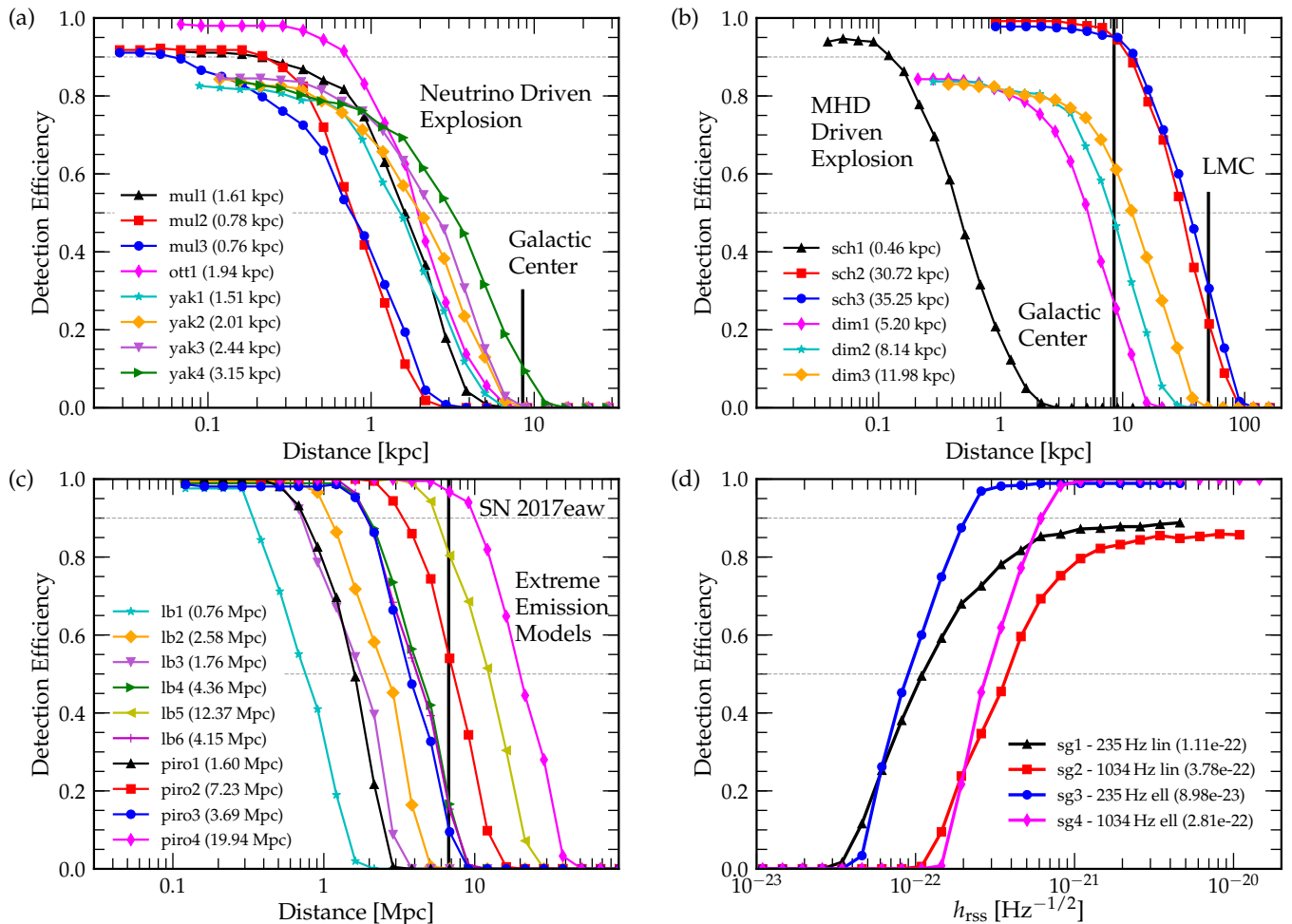


FIG. 5. Panels (a), (b), and (c) show the efficiency as a function of distance using 3 families of waveforms for a source located at the position and time of SN 2017eaw. Panel (d) provides the detection efficiency for *ad hoc* sine-Gaussian waveforms as a function of h_{rss} , which we use to constrain GW energy and discuss in Sec. VB. The numbers in parentheses for the models plotted in (a), (b), and (c) are the distances at which the detection efficiency equals 50%. For (d), the numbers in parentheses are the h_{rss} values resulting in 50% detection efficiencies. The detection reach for neutrino-driven explosions is limited to a few kpc while for magnetorotationally-driven (MHD-driven) explosions it covers the Milky Way and the detection efficiency at the distance of the Large Magellanic Cloud (LMC), that hosted SN 1987A, is non-zero. Further discussion can be found in Sec. VA. The distance reaches for extreme emission models in (c) exceed the distance of SN 2017eaw. Given that there was no GW detection, we are able to exclude some of the parameter spaces for these models, which we discuss in Sec. VC. The dashed lines show 50% and 90% detection efficiencies.

In Table VIII, we report GW energy constraints for each CCSN. For the *ad hoc* waveforms with peak frequency at 235 Hz (sg1 and sg3), the GW energy constraints are consistently on the order of $10^{-3} M_{\odot} c^2$ or less. The lowest achieved energy constraints are obtained for SN 2017eaw at low frequency, $4.27 \times 10^{-4} M_{\odot} c^2$ (7.63×10^{50} erg), and high frequency, $1.28 \times 10^{-1} M_{\odot} c^2$ (2.30×10^{53} erg). For both low and high frequency emission, the energy constraints are two orders of magnitude stronger than in the search with the initial interferometer data [35]. This improvement is due to the improved sensitivity of the detectors and the closer distance of SN 2017eaw (6.72 Mpc) in comparison to SN 2007gr (10.55 Mpc). However, these energy constraints are still a few orders of magnitude larger than the energies pre-

dicted from multidimensional simulations (Table III), that lie between around $10^{-11} M_{\odot} c^2$ and $10^{-7} M_{\odot} c^2$.

The GW energy constraints obtained in this search can be compared to the energy budget of a CCSN. The energy available during collapse is approximately the gravitational binding energy of the final neutron star remnant, which is typically $1.5 \times 10^{-1} M_{\odot} c^2$ (3×10^{53} erg, [120–122]). Around 99% of that energy is radiated via neutrinos during the cooling of the proto-neutron star [123] and the remaining $\sim 1\%$ is mainly transferred into kinetic energy. In a realistic scenario, only a small fraction of the explosion’s energy is radiated in the GW spectrum (Sec. IV C).

In Sec. IV C we describe several processes emitting GWs. Some of them (e.g., SASI and convection) are

TABLE VI. Distance reaches (in kpc), defined as the distance with a 50% detection efficiency, for neutrino-driven explosions from Müller (mul1-mul3), Ott (ott1) and Yakunin (yak1-yak4), as well as MHD-driven explosions from Scheidegger (sch1-sch3) and Dimmelmeier (dim1-dim3).

Supernova	mul1	mul2	mul3	ott1	yak1	yak2	yak3	yak4	sch1	sch2	sch3	dim1	dim2	dim3
SN 2015as	1.53	0.84	0.97	2.20	1.73	1.89	2.05	2.47	0.49	34.76	41.32	5.57	7.34	14.06
SN 2016B	1.32	0.70	0.58	1.74	0.65	1.07	1.32	2.12	0.40	26.66	34.88	3.82	5.24	12.09
SN 2016X	1.26	0.57	0.66	1.72	0.50	0.84	0.81	1.62	0.37	26.02	32.13	2.52	3.80	10.22
SN 2017eaw	1.61	0.78	0.76	1.94	1.51	2.01	2.44	3.15	0.46	30.72	35.25	5.20	8.14	11.98
SN 2017gax	2.40	1.15	1.24	3.09	2.30	2.75	2.95	5.08	0.65	42.29	53.55	8.04	10.19	22.35

TABLE VII. Distance reaches (in Mpc), defined as the distance with a 50% detection efficiency, for extreme emission models Torus Fragmentation Instability (piro1-piro4) and Long-lasting Bar Mode (lb1-lb6).

Supernova	piro1	piro2	piro3	piro4	lb1	lb2	lb3	lb4	lb5	lb6
SN 2015as	1.33	7.13	3.83	19.70	0.93	2.93	1.92	4.59	15.24	4.86
SN 2016B	1.31	7.04	3.47	17.94	0.80	2.64	1.80	4.24	13.69	4.50
SN 2016X	1.32	6.86	3.20	19.55	0.73	2.36	1.46	3.83	12.16	3.73
SN 2017eaw	1.60	7.23	3.69	19.94	0.76	2.58	1.76	4.36	12.37	4.15
SN 2017gax	1.81	10.04	5.22	27.79	1.23	3.55	2.63	6.16	19.03	6.40

related to the movement of matter that is ejected during an explosion. Again, according to the multidimensional simulations, only a small portion of this energy is converted into GWs. The kinetic energy of CCSN ejecta is typically on the order of $5.5 \times 10^{-4} M_{\odot} c^2$ (10^{51} erg) [124–126]. Specifically, estimates of the kinetic energy in the ejecta of SN 2015as and SN 2017eaw are $2.5 \times 10^{-3} M_{\odot} c^2$ (4.4×10^{51} erg) [49] and $1.1 \times 10^{-3} M_{\odot} c^2$ (2.0×10^{51} erg) [58], respectively. The current GW constraints at low frequencies are comparable with these values. Specifically, the low frequency (235 Hz) constraints for SN 2017eaw are roughly an order of magnitude below the kinetic energy of CCSN ejecta.

For extreme emission models, the GW energies are orders of magnitude larger than those predicted for multidimensional simulations, as seen in Table IV. The energies of these extreme emission processes range from $2.98 \times 10^{-4} M_{\odot} c^2$ up to even $1.18 \times 10^{-1} M_{\odot} c^2$. Our energy constraints are comparable with these values, but the comparison would not be correct as the *ad hoc* signals and the extreme emission model waveforms frequency content are different.

C. Model exclusion statements for extreme emission models

Along with constraining the GW energy emitted by CCSNe, we also constrain two models of extreme GW emission. As described in Sec. V A, for a few waveforms of the extreme emission models, the distance reaches exceed the distances of the CCSNe analyzed in this search. Given no GW detection, these models most likely do not

describe correctly the CCSN explosion phenomena. Similarly to Ref. [35], we consider a *standard candle* approach, that is we assume that each CCSN emits an identical GW signal. To characterize the models, we use waveforms that probe sample regions of the parameter spaces of these models (see Table IV and Sec. IV C 2).

The method for excluding models from multiple astrophysical sources is described in detail in [127]. In this method we use the detection efficiency, $\mathcal{E}(d)$, which is a function of the distance, d . If a GW transient is strong and detectable but arrives at the detectors when coincident data is not available, then the model that predicts such a transient cannot be excluded. Therefore, we need to take into account the coincident duty factor, $a \in [0, 1]$. We define the *reduced detection efficiency* as

$$\epsilon(d) = a \times \mathcal{E}(d). \quad (4)$$

Given no GW detection, the reduced detection efficiency can also be understood as a model exclusion probability. For example, the detection efficiency for the piro4 waveform reaches 96.7% (see Figure 5) at the distance of SN 2017eaw (6.72 Mpc). When we take into account the effect of the 48.8% coincident duty factor for this CCSN (see Table I) the reduced detection efficiency is 47.2%. Hence we are confident with 47% probability that the piro4 model does not correctly describe the nature of a CCSN engine.

We then combine model exclusion probabilities obtained for each CCSN by multiplying the probabilities of not detecting a signal. The overall model exclusion

TABLE VIII. Gravitational-wave energy emission constraints at 50% detection efficiency. We assumed isotropic GW emission for the four *ad hoc* waveforms. The most stringent constraints (in bold) are achieved for the closest event, SN 2017eaw (6.72 Mpc). They are two orders of magnitude smaller than the results obtained in Ref. [35]. The energies obtained for 235 Hz emission are comparable to the typical explosion energy ($\sim 10^{51}$ erg) and a typical kinetic energy of CCSN ejecta ($\sim 10^{51}$ erg).

Supernova	Quantity	sg1 - 235 Hz lin	sg2 - 1304 Hz lin	sg3 - 235 Hz ell	sg4 - 1304 Hz ell
SN 2015as	h_{rssi} [Hz $^{-1/2}$]	8.96e-23	2.95e-22	7.72e-23	2.58e-22
	E_{GW} [erg]	6.20e+51	2.07e+54	4.60e+51	1.58e+54
	E_{GW} [$M_{\odot}c^2$]	3.47e-03	1.16e+00	2.57e-03	8.82e-01
SN 2016B	h_{rssi} [Hz $^{-1/2}$]	1.15e-22	4.07e-22	8.72e-23	2.71e-22
	E_{GW} [erg]	9.59e+51	3.70e+54	5.51e+51	1.64e+54
	E_{GW} [$M_{\odot}c^2$]	5.37e-03	2.07e+00	3.08e-03	9.15e-01
SN 2016X	h_{rssi} [Hz $^{-1/2}$]	1.33e-22	4.52e-22	9.86e-23	3.11e-22
	E_{GW} [erg]	8.60e+51	3.05e+54	4.70e+51	1.44e+54
	E_{GW} [$M_{\odot}c^2$]	4.81e-03	1.71e+00	2.63e-03	8.08e-01
SN 2017eaw	h_{rssi} [Hz $^{-1/2}$]	1.11e-22	3.78e-22	8.98e-23	2.81e-22
	E_{GW} [erg]	1.16e+51	4.17e+53	7.63e+50	2.30e+53
	E_{GW} [$M_{\odot}c^2$]	6.49e-04	2.33e-01	4.27e-04	1.28e-01
SN 2017gax	h_{rssi} [Hz $^{-1/2}$]	6.80e-23	2.35e-22	5.72e-23	1.98e-22
	E_{GW} [erg]	3.76e+51	1.38e+54	2.66e+51	9.79e+53
	E_{GW} [$M_{\odot}c^2$]	2.10e-03	7.71e-01	1.49e-03	5.47e-01

probability

$$P_{\text{excl}} = 1 - \prod_{i=1}^N (1 - \epsilon_i(d_i)), \quad (5)$$

where N is the number of CCSNe.

The results for the ten waveforms described in Sec. IV C 2 are shown in Table IX. The greatest $P_{\text{excl}} = 83.2\%$ is obtained for the piro4 waveform and the largest contributions come from SN 2017eaw and SN 2017gax because the detection ranges for these CCSNe are larger than their distances. Although SN 2017eaw makes the most important contribution to the model exclusion statements, the most energetic models, piro4 and lb5, are constrained by all CCSNe.

For the Torus Fragmentation Instability model, the waveforms are characterized by the mass of a central black hole and the thickness of a torus around it. The clump masses M_f for the piro1-piro4 waveforms are $0.072 M_{\odot}$, $0.576 M_{\odot}$, $0.144 M_{\odot}$, $1.152 M_{\odot}$ respectively. There is a correlation between the mass of the fragment and P_{excl} because the amplitude of the waveform scales approximately with M_f . We conclude that if central black holes are created in type-II and type-Ib/c supernovae after core-collapse, then any clumps formed by fragmentation are preferably small ($M_f \lesssim 1M_{\odot}$). Moreover, if the torii are created around black holes, they are either non-fragmented or rather thin, for the disk model considered in Ref. [101].

For the Long-Lasting Bar Mode model, the parameter space is larger than for the Torus Fragmentation Instability model. Three models have non-zero P_{excl} values, lb4, lb5, and lb6. All three models have large values of

$M(L^2 - 3R^2) = 3300 M_{\odot}\text{km}^2$, which corresponds either to $R \leq 10$ km proto-neutron stars with large asymmetries ($L/2R > 2.5$) or large proto-neutron stars ($R \approx 20$ km) with moderate asymmetries ($L/2R \approx 1.5 - 3.5$). If bars are created generically in type-II and type-Ib/c supernovae, the deformations are preferably small. The largest P_{excl} among these models is obtained for lb5. This waveform lasts 1 s, while lb4 and lb6 are 100 ms and 25 ms respectively. It seems that, for a proto-neutron star with $R \leq 10$ km, if bars with strong deviations from axisymmetry are created ($L/2R > 3$) in CCSNe, then they are rather short lived. Larger proto-neutron stars ($R \approx 20$ km) could still have large deformations and be unobservable.

The constraint for lb5 limits the possible maximum deformations in type-II and type-Ib/c supernovae. If bars are created they are probably small. In case deformations are large the proto-neutron star is either very compact ($R \sim 5$ km) or the bar is short lived (< 1000 ms). These results are consistent with the current theoretical understanding of bar-mode instabilities, which are expected to appear early after bounce when the proto-neutron star mass is relatively low ($M \leq 1 M_{\odot}$) and its radius large ($R \geq 20$ km). The amplitude and duration are also expected to be severely limited by the presence of strong magnetic fields, magneto-rotational turbulence, and shear instabilities.

VI. SUMMARY AND DISCUSSION

We present the results of a search for GWs from CCSNe with the Advanced LIGO and Advanced Virgo de-

TABLE IX. Model Exclusion Probabilities (P_{excl}) for extreme emission models with a standard candle approach (see Sec. V C for details of the method). We infer that if bars are created generically in type-II and type-Ib/c supernovae, then the deformations are preferably small. If central black holes are created in CCSN, then the accretion tori around them are either non-fragmented or rather thin.

Supernova		piro1	piro2	piro3	piro4	lb1	lb2	lb3	lb4	lb5	lb6
Reduced Detection Efficiency ϵ [%]	SN 2015as	0.0	0.2	0.0	18.0	0.0	0.0	0.0	0.0	8.4	0.0
	SN 2016B	0.0	0.1	0.0	16.0	0.0	0.0	0.0	0.0	5.5	0.0
	SN 2016X	0.0	0.0	0.0	9.8	0.0	0.0	0.0	0.0	3.1	0.0
	SN 2017eaw	0.0	26.8	5.2	47.2	0.0	0.0	0.0	8.7	39.5	8.0
	SN 2017gax	0.0	0.2	0.0	48.7	0.0	0.0	0.0	0.0	28.6	0.0
P_{excl} [%]		0.0	27.2	5.2	83.2	0.0	0.0	0.0	8.7	63.8	8.0

tectors during the first and second observing runs (2015-2017). Five CCSNe within 20 Mpc are used for the astrophysical statements: SN 2015as, SN 2016B, SN 2016X, SN 2017eaw, and SN 2017gax. We have not found any significant GW candidate. All the loudest events are consistent with background events.

We provide the distance reaches at 50% detection efficiencies for both realistic and extreme GW emission models. For the neutrino driven explosions the distances do not exceed 5 kpc, while the distance ranges for the magnetorotationally driven explosions reach 54 kpc. The distance reaches for extreme emission models can be as large as 28 Mpc, which exceed the distances of CCSNe analyzed in this search. Given no GW detection, this gives us an opportunity to estimate the exclusion probabilities for the most extreme models.

We derive GW energy constraints for generic low and high frequency GW emissions at 235 Hz and 1304 Hz respectively using linearly and elliptically polarized *ad-hoc* sine-Gaussian waveforms. The constraints are around $10^{-3} M_{\odot}c^2$ and $10^{-1} M_{\odot}c^2$ for low and high frequency GW emission, respectively. The best GW emission constraints we obtained are for SN 2017eaw of $4.27 \times 10^{-4} M_{\odot}c^2$ (7.63×10^{50} erg) for low frequency emission and $1.28 \times 10^{-1} M_{\odot}c^2$ (2.30×10^{53} erg) for high frequency emission. These are two orders of magnitude more stringent than in [35], but still a few orders of magnitude larger than predicted from multidimensional simulations. The low frequency emission constraints are comparable to the typical kinetic energy of CCSN ejecta.

We provide the first supernova model constraints based on O1 and O2 data with a standard candle approach. The most extreme emission models, piro4 and lb5, are constrained at the level of 83.2% and 63.8% respectively. Out of ten waveforms, we place limits on six of them with 5% to 83% exclusion probabilities. Based on our results, we conclude that if central black holes are created in type-II and type-Ib/c supernovae, the sizes of the fragments are preferably small. Moreover, if disks around central black holes are created, then they are either non-fragmented or rather thin. If bars are created, they are probably small. In cases where deformations of the proto-neutron star are large, they are either very

compact ($R \sim 5$ km) or they shortly lived (< 1000 ms).

These model exclusion statements are the first constraints on CCSN engines based on GW data. In the future, with targeted searches and upgraded detectors (third observing run and beyond) it will be possible to further exclude the extreme emission models and better constrain the GW energy emitted by CCSN engines, making both more astrophysically meaningful.

ACKNOWLEDGMENTS

The authors gratefully acknowledge the support of the United States National Science Foundation (NSF) for the construction and operation of the LIGO Laboratory and Advanced LIGO as well as the Science and Technology Facilities Council (STFC) of the United Kingdom, the Max-Planck-Society (MPS), and the State of Niedersachsen/Germany for support of the construction of Advanced LIGO and construction and operation of the GEO600 detector. Additional support for Advanced LIGO was provided by the Australian Research Council. The authors gratefully acknowledge the Italian Istituto Nazionale di Fisica Nucleare (INFN), the French Centre National de la Recherche Scientifique (CNRS) and the Foundation for Fundamental Research on Matter supported by the Netherlands Organisation for Scientific Research, for the construction and operation of the Virgo detector and the creation and support of the EGO consortium. The authors also gratefully acknowledge research support from these agencies as well as by the Council of Scientific and Industrial Research of India, the Department of Science and Technology, India, the Science & Engineering Research Board (SERB), India, the Ministry of Human Resource Development, India, the Spanish Agencia Estatal de Investigación, the Vicepresidència i Conselleria d’Innovació, Recerca i Turisme and the Conselleria d’Educació i Universitat del Govern de les Illes Balears, the Conselleria d’Educació, Investigació, Cultura i Esport de la Generalitat Valenciana, the National Science Centre of Poland, the Swiss National Science Foundation (SNSF), the Russian Foundation for Basic Research, the Russian Science Foundation, the European Commission,

the European Regional Development Funds (ERDF), the Royal Society, the Scottish Funding Council, the Scottish Universities Physics Alliance, the Hungarian Scientific Research Fund (OTKA), the Lyon Institute of Origins (LIO), the Paris Île-de-France Region, the National Research, Development and Innovation Office Hungary (NKFIH), the National Research Foundation of Korea, Industry Canada and the Province of Ontario through the Ministry of Economic Development and Innovation, the Natural Science and Engineering Research Council Canada, the Canadian Institute for Advanced Research, the Brazilian Ministry of Science, Technology, Innovations, and Communications, the International Center for Theoretical Physics South American Institute for Fundamental Research (ICTP-SAIFR), the Research Grants Council of Hong Kong, the National Natural Science Foundation of China (NSFC), the Leverhulme Trust, the Research Corporation, the Ministry of Science and Technology (MOST), Taiwan and the Kavli Foundation. The authors gratefully acknowledge the support of the NSF, STFC, INFN and CNRS for provision of computational

resources. Research by DJS is supported by NSF grants AST-1821987, AST-1821967, AST-1813708, and AST-1813466. We thank the Las Cumbres Observatory (LCO) and its staff for its continuing support of the ASAS-SN project. ASAS-SN is supported by the Gordon and Betty Moore Foundation through grant GBMF5490 to the Ohio State University and NSF grant AST-1515927. Development of ASAS-SN has been supported by NSF grant AST-0908816, the Mt. Cuba Astronomical Foundation, the Center for Cosmology and AstroParticle Physics at the Ohio State University, the Chinese Academy of Sciences South America Center for Astronomy (CASSACA), the Villum Foundation, and George Skestos. KZS and CSK are supported by NSF grants AST-1515876, AST-1515927, and AST-1814440. Support for JLP is provided in part by FONDECYT through the grant 1191038 and by the Ministry of Economy, Development, and Tourism's Millennium Science Initiative through grant IC120009, awarded to The Millennium Institute of Astrophysics, MAS. Research by SV is supported by NSF grants AST-1813176. This document has been assigned LIGO Laboratory document number LIGO-P1700177.

-
- [1] B. P. Abbott *et al.* (LIGO Scientific Collaboration and Virgo Collaboration), *Phys. Rev. Lett.* **116**, 061102 (2016), [arXiv:1602.03837 \[gr-qc\]](#).
- [2] B. P. Abbott *et al.* (LIGO Scientific Collaboration and Virgo Collaboration), Submitted to *Phys. Rev. X* (2018), [arXiv:1811.12907 \[astro-ph.HE\]](#).
- [3] B. P. Abbott *et al.* (LIGO Scientific Collaboration and Virgo Collaboration), *Physical Review X* **6**, 041015 (2016), [arXiv:1606.04856 \[gr-qc\]](#).
- [4] B. P. Abbott *et al.* (LIGO Scientific Collaboration and Virgo Collaboration), *Phys. Rev. Lett.* **116**, 241103 (2016), [arXiv:1606.04855 \[gr-qc\]](#).
- [5] B. P. Abbott *et al.* (LIGO Scientific Collaboration and Virgo Collaboration), *Phys. Rev. Lett.* **118**, 221101 (2017), [arXiv:1706.01812 \[gr-qc\]](#).
- [6] B. P. Abbott *et al.* (LIGO Scientific Collaboration and Virgo Collaboration), *Phys. Rev. Lett.* **119**, 141101 (2017), [arXiv:1709.09660 \[gr-qc\]](#).
- [7] B. P. Abbott *et al.* (LIGO Scientific Collaboration and Virgo Collaboration), *Astrophys. J.* **851**, L35 (2017), [arXiv:1711.05578 \[astro-ph.HE\]](#).
- [8] B. Abbott *et al.* (LIGO Scientific Collaboration and Virgo Collaboration), *Phys. Rev. Lett.* **119**, 161101 (2017), [arXiv:1710.05832 \[gr-qc\]](#).
- [9] B. P. Abbott *et al.* (LIGO Scientific, Virgo, Fermi GBM, INTEGRAL, IceCube, AstroSat Cadmium Zinc Telluride Imager Team, IPN, Insight-Hxmt, ANTARES, Swift, AGILE Team, 1M2H Team, Dark Energy Camera GW-EM, DES, DLT40, GRAWITA, Fermi-LAT, ATCA, ASKAP, Las Cumbres Observatory Group, OzGrav, DWF (Deeper Wider Faster Program), AST3, CAASTRO, VINROUGE, MASTER, J-GEM, GROWTH, JAGWAR, CaltechNRAO, TTU-NRAO, NuSTAR, Pan-STARRS, MAXI Team, TZAC Consortium, KU, Nordic Optical Telescope, ePESSTO, GROND, Texas Tech University, SALT Group, TOROS, BOOTES, MWA, CALET, IKI-GW Follow-up, H.E.S.S., LOFAR, LWA, HAWC, Pierre Auger, ALMA, Euro VLBI Team, Pi of Sky, Chandra Team at McGill University, DFN, ATLAS Telescopes, High Time Resolution Universe Survey, RIMAS, RATIR, SKA South Africa/MeerKAT), *Astrophys. J.* **848**, L12 (2017), [arXiv:1710.05833 \[astro-ph.HE\]](#).
- [10] B. P. Abbott *et al.* (LIGO Scientific Collaboration and Virgo Collaboration), *Astrophys. J.* **875**, 161 (2019), [arXiv:1901.03310 \[astro-ph.HE\]](#).
- [11] B. P. Abbott *et al.* (LIGO Scientific, Virgo, Fermi-GBM, INTEGRAL), *Astrophys. J.* **848**, L13 (2017), [arXiv:1710.05834 \[astro-ph.HE\]](#).
- [12] D. A. Coulter *et al.*, *Science* **358**, 1556 (2017), [arXiv:1710.05452 \[astro-ph.HE\]](#).
- [13] B. Abbott *et al.* (LIGO Scientific and Virgo and 1M2H and Dark Energy Camera GW-EM and DES and DLT40 and Las Cumbres Observatory and VINROUGE and MASTER), *Nature* **551**, 85 (2017), [arXiv:1710.05835 \[astro-ph.CO\]](#).
- [14] K. Hirata, T. Kajita, M. Koshiba, M. Nakahata, and Y. Oyama, *Phys. Rev. Lett.* **58**, 1490 (1987).
- [15] R. M. Bionta, G. Blewitt, C. B. Bratton, D. Casper, and A. Ciocio, *Phys. Rev. Lett.* **58**, 1494 (1987).
- [16] E. N. Alekseev, L. N. Alekseeva, I. V. Krivosheina, and V. I. Volchenko, *European Southern Observatory Conference and Workshop Proceedings*, European Southern Observatory Conference and Workshop Proceedings, **26**, 237 (1987).
- [17] A. Burrows, J. Hayes, and B. A. Fryxell, *Astrophys. J.* **450**, 830 (1995), [arXiv:astro-ph/9506061](#).
- [18] M. Herant, *Phys. Rep.* **256**, 117 (1995).
- [19] S. M. Couch and C. D. Ott, *Astrophys. J.* **799**, 5 (2015), [arXiv:1408.1399 \[astro-ph.HE\]](#).

- [20] E. J. Lentz *et al.*, *Astrophys. J. Lett.* **807**, L31 (2015), [arXiv:1505.05110 \[astro-ph.SR\]](#).
- [21] H.-T. Janka, *Ann. Rev. Nuc. Par. Sci.* **62**, 407 (2012), [arXiv:1206.2503 \[astro-ph.SR\]](#).
- [22] H.-T. Janka, in *Handbook of Supernovae* (Springer International Publishing, 2017) pp. 1095–1150.
- [23] B. Müller, *Publications of the Astronomical Society of Australia* **33**, e048 (2016), [arXiv:1608.03274 \[astro-ph.SR\]](#).
- [24] S. van den Bergh and G. A. Tammann, *Ann. Rev. Astron. Astroph.* **29**, 363 (1991).
- [25] E. Cappellaro, M. Turatto, S. Benetti, D. Y. Tsvetkov, O. S. Bartunov, and I. N. Makarova, *Astron. Astrophys.* **273**, 383 (1993), [arXiv:astro-ph/9302017](#).
- [26] G. A. Tammann, W. Loeffler, and A. Schroeder, *Astrophys. J. Supp. Ser.* **92**, 487 (1994).
- [27] W. Li *et al.*, *Mon. Not. Roy. Astron. Soc.* **412**, 1441 (2011), [arXiv:1006.4612 \[astro-ph.SR\]](#).
- [28] R. Diehl *et al.*, *Nature* **439**, 45 (2006), [arXiv:astro-ph/0601015](#).
- [29] D. Maoz and C. Badenes, *Mon. Not. Roy. Astron. Soc.* **407**, 1314 (2010), [arXiv:1003.3031 \[astro-ph.GA\]](#).
- [30] S. M. Adams, C. S. Kochanek, J. F. Beacom, M. R. Vagins, and K. Z. Stanek, *Astrophys. J.* **778**, 164 (2013), [arXiv:1306.0559 \[astro-ph.HE\]](#).
- [31] J. Abadie *et al.* (LIGO Scientific Collaboration and Virgo Collaboration), *Phys. Rev. D* **85**, 122007 (2012), [arXiv:1202.2788 \[gr-qc\]](#).
- [32] J. Abadie *et al.* (LIGO Scientific Collaboration and Virgo Collaboration), *Phys. Rev.* **D81**, 102001 (2010), [arXiv:1002.1036 \[gr-qc\]](#).
- [33] B. P. Abbott *et al.* (LIGO Scientific Collaboration and Virgo Collaboration), *Physical Review D* **95**, 042003 (2017), [arXiv:1611.02972 \[gr-qc\]](#).
- [34] B. P. Abbott *et al.* (LIGO Scientific Collaboration and Virgo Collaboration), *Phys. Rev. D* **100**, 024017 (2019), [arXiv:1905.03457 \[gr-qc\]](#).
- [35] B. P. Abbott *et al.* (LIGO Scientific Collaboration and Virgo Collaboration), *Phys. Rev. D* **94**, 102001 (2016), [arXiv:1605.01785 \[gr-qc\]](#).
- [36] R. E. Rutledge, *Publications of the Astronomical Society of the Pacific* **110**, 754 (1998).
- [37] B. J. Shappee *et al.*, *The Astrophysical Journal* **788**, 48 (2014), [arXiv:1310.2241 \[astro-ph.HE\]](#).
- [38] T. W.-S. Holoiien *et al.*, *Monthly Notices of the Royal Astronomical Society* **484**, 1899 (2019), [arXiv:1811.08904 \[astro-ph.HE\]](#).
- [39] D. Godoy-Rivera *et al.*, *Monthly Notices of the Royal Astronomical Society* **471**, 4966 (2017), [arXiv:1704.02320 \[astro-ph.HE\]](#).
- [40] D. Godoy-Rivera *et al.*, *Monthly Notices of the Royal Astronomical Society* **467**, 1098 (2017), [arXiv:1610.03061 \[astro-ph.HE\]](#).
- [41] L. Tartaglia *et al.*, *The Astronomer’s Telegram* **10638** (2017).
- [42] T. Prusti *et al.* (Gaia Collaboration), *Astron. Astrophys.* **595**, A1 (2016), [arXiv:1609.04153 \[astro-ph.IM\]](#).
- [43] A. G. A. Brown *et al.* (Gaia Collaboration), *Astron. Astrophys.* **595**, A2 (2016), [arXiv:1609.04172 \[astro-ph.IM\]](#).
- [44] “ASRAS,” [www.rochesterastronomy.org](#) (2018), accessed: 2018-07-29.
- [45] L. Tartaglia *et al.*, *Astrophys. J.* **853**, 62 (2018), [arXiv:1711.03940 \[astro-ph.HE\]](#).
- [46] J. Guillochon, J. Parrent, L. Z. Kelley, and R. Margutti, *Astrophys. J.* **835**, 64 (2017), [arXiv:1605.01054 \[astro-ph.SR\]](#).
- [47] “CBAT,” <http://www.cbateps.harvard.edu/cbat.html> (2018), accessed: 2018-07-29.
- [48] L. Tartaglia *et al.*, *The Astronomer’s Telegram* **8291** (2015).
- [49] A. Gangopadhyay *et al.*, Accepted by *Monthly Notices of the Royal Astronomical Society* (2018), [arXiv:1802.06731 \[astro-ph.HE\]](#).
- [50] A. Gangopadhyay *et al.*, *Bulletin de la Societe Royale des Sciences de Liege* **87**, 351 (2018).
- [51] B. J. Shappee *et al.*, *The Astronomer’s Telegram* **8502** (2016).
- [52] C. P. Gutiérrez *et al.*, *Mon. Not. Roy. Astron. Soc.* **479**, 3232 (2018), [arXiv:1806.03855 \[astro-ph.HE\]](#).
- [53] G. Bock *et al.*, *The Astronomer’s Telegram* **8566** (2016).
- [54] F. Huang *et al.*, *Monthly Notices of the Royal Astronomical Society* **475**, 3959 (2018), [arXiv:1801.03167 \[astro-ph.HE\]](#).
- [55] S. Dong and K. Z. Stanek, *The Astronomer’s Telegram* **10372** (2017).
- [56] N. A. Tikhonov, *Astronomy Letters* **40**, 537 (2014).
- [57] C. D. Kilpatrick and R. J. Foley, *Monthly Notices of the Royal Astronomical Society* **481**, 2536 (2018), [arXiv:1806.00348 \[astro-ph.SR\]](#).
- [58] D. Y. Tsvetkov *et al.*, *Astronomy Letters* **44**, 315 (2018), [arXiv:1801.00340 \[astro-ph.HE\]](#).
- [59] S. Tinyanont *et al.*, *The Astrophysical Journal* **873**, 127 (2019), [arXiv:1901.01940 \[astro-ph.HE\]](#).
- [60] “The Open Supernova Catalog: SN 2017gax,” <https://sne.space/sne/2017gax/> (2018), accessed: 2018-12-02.
- [61] “Transient Name Server: SN 2016C,” <https://sne.space/sne/2016C/> (2018), accessed: 2018-12-02.
- [62] D. K. Sahu *et al.*, *The Astronomer’s Telegram* **8514** (2016).
- [63] “The Open Supernova Catalog: SN2017ein,” <https://sne.space/sne/SN2017ein/> (2018), accessed: 2018-12-02.
- [64] D. Xiang *et al.*, *Astrophys. J.* **871**, 176 (2019), [arXiv:1812.03076 \[astro-ph.HE\]](#).
- [65] “The Open Supernova Catalog: SN2017aym,” <https://sne.space/sne/SN2017aym/> (2018), accessed: 2018-12-02.
- [66] A. Delgado *et al.*, *Transient Name Server Discovery Report* **2017-214** (2017).
- [67] “The Open Supernova Catalog: SN2017bzb,” <https://sne.space/sne/SN2017bzb/> (2018), accessed: 2018-12-02.
- [68] S. Parker, *Transient Name Server Discovery Report* **2017-279** (2017).
- [69] E. Waxman and B. Katz, “Shock breakout theory,” in *Handbook of Supernovae*, edited by A. W. Alsabti and P. Murdin (Springer International Publishing, Cham, 2017) pp. 1–49.
- [70] A. Gal-Yam *et al.*, *Nature* **509**, 471 (2014).
- [71] S. J. Smartt, *Astrophysics and Space Science* **281**, 187 (2002).
- [72] S. D. V. Dyk, *Philosophical Transactions of the Royal Society A: Mathematical, Physical and Engineering Sciences* **375**, 20160277 (2017).
- [73] J. J. Eldridge, (2006), [arXiv:astro-ph/0612477](#).

- [74] L.-X. Li, *Monthly Notices of the Royal Astronomical Society* **375**, 240 (2007).
- [75] S. J. Smartt, *Ann. Rev. Astron. Astroph.* **47**, 63 (2009).
- [76] B. Davies, *Philosophical Transactions of the Royal Society A: Mathematical, Physical and Engineering Sciences* **375**, 20160270 (2017).
- [77] K. Schawinski *et al.*, *Science* **321**, 223 (2008), [arXiv:0803.3596 \[astro-ph\]](#).
- [78] L. Dessart, D. John Hillier, and E. Audit, *Astron. Astrophys.* **605**, A83 (2017), [arXiv:1704.01697 \[astro-ph.SR\]](#).
- [79] K. Gill and M. Zanolin, *LIGO Document Control Center* (2017).
- [80] E. Waxman and B. Katz, in *Handbook of Supernovae* (Springer International Publishing, 2017) pp. 967–1015, [arXiv:1607.01293 \[astro-ph.HE\]](#).
- [81] J. Vinkó and K. Takáts, *Supernova 1987A: 20 Years After: Supernovae and Gamma-Ray Bursters*, *American Institute of Physics Conference Series*, **937**, 394 (2007), [arXiv:0704.0552](#).
- [82] S. Bose and B. Kumar, *Astrophys. J.* **782**, 98 (2014), [arXiv:1401.5115](#).
- [83] J. Emilio Enriquez *et al.*, in *American Astronomical Society Meeting Abstracts #217*, *Bulletin of the American Astronomical Society*, Vol. 43 (2011) p. 337.21.
- [84] D. C. Leonard, L. Dessart, D. J. Hillier, and G. Pignata, in *American Institute of Physics Conference Series*, *American Institute of Physics Conference Series*, Vol. 1429, edited by J. L. Hoffman, J. Bjorkman, and B. Whitney (2012) pp. 204–207, [arXiv:1109.5406 \[astro-ph.SR\]](#).
- [85] V. Morozova *et al.*, *Astrophys. J.* **814**, 63 (2015), [arXiv:1505.06746 \[astro-ph.HE\]](#).
- [86] B. P. Abbott *et al.* (LIGO Scientific Collaboration and Virgo Collaboration), *Classical and Quantum Gravity* **33**, 134001 (2016).
- [87] B. P. Abbott *et al.* (LIGO Scientific Collaboration and Virgo Collaboration), *Physical Review D* **93**, 122004 (2016).
- [88] L. K. Nuttall, *Philosophical Transactions of the Royal Society A: Mathematical, Physical and Engineering Sciences* **376**, 20170286 (2018).
- [89] S. E. Gossan, P. Sutton, A. Stuver, M. Zanolin, K. Gill, and C. D. Ott, *Phys. Rev. D* **93**, 042002 (2016).
- [90] M. J. Szczepańczyk and C. D. Ott, *Expressing gravitational waves energy in terms of quadrupole moment*, *Tech. Rep. LIGO-T1500586* (2015).
- [91] E. Müller, H.-T. Janka, and A. Wongwathanarat, *Astron. Astrophys.* **537**, A63 (2012), [arXiv:1106.6301 \[astro-ph.SR\]](#).
- [92] C. D. Ott *et al.*, *Astrophys. J.* **768**, 115 (2013), [arXiv:1210.6674 \[astro-ph.HE\]](#).
- [93] K. N. Yakunin *et al.*, Submitted to *Phys. Rev. D.* (2015), [arXiv:1505.05824 \[astro-ph.HE\]](#).
- [94] S. Scheidegger, R. Käppeli, S. C. Whitehouse, T. Fischer, and M. Liebendörfer, *Astron. Astrophys.* **514**, A51 (2010), [arXiv:1001.1570 \[astro-ph.HE\]](#).
- [95] H. Dimmelmeier, C. D. Ott, A. Marek, and H.-T. Janka, *Phys. Rev. D.* **78**, 064056 (2008).
- [96] S. Klimentenko *et al.*, *Phys. Rev. D* **93**, 042004 (2016), [arXiv:1511.05999 \[gr-qc\]](#).
- [97] M. Cabero *et al.*, (2019), [arXiv:1901.05093 \[physics.ins-det\]](#).
- [98] J. Abadie *et al.* (LIGO Scientific Collaboration and Virgo Collaboration), *Nuclear Instruments and Methods in Physics Research Section A: Accelerators, Spectrometers, Detectors and Associated Equipment* **624**, 223 (2010).
- [99] T. Accadia, F. Acernese, M. Alshourbagy, P. Amico, F. Antonucci, S. Aoudia, N. Arnaud, C. Arnault, K. G. Arun, P. Astone, and *et al.*, *Journal of Instrumentation* **7**, 3012 (2012).
- [100] C. D. Ott, *GWs from Barmode Instabilities*, *Tech. Rep. LIGO-T1000553-v2* (LIGO Scientific Collaboration, 2010).
- [101] A. L. Piro and E. Pfahl, *Astrophys. J.* **658**, 1173 (2007).
- [102] A. Mezzacappa *et al.*, (2015), [arXiv:1501.01688 \[astro-ph.SR\]](#).
- [103] K. Kotake, N. Ohnishi, and S. Yamada, *Astrophys. J.* **655**, 406 (2007).
- [104] T. Foglizzo *et al.*, *Publications of the Astronomical Society of Australia* **32**, e009 (2015), [arXiv:1501.01334 \[astro-ph.HE\]](#).
- [105] P. Cerdá-Durán, N. DeBrye, M. A. Aloy, J. A. Font, and M. Obergaulinger, *The Astrophysical Journal* **779**, L18 (2013).
- [106] V. Morozova, D. Radice, A. Burrows, and D. Vartanyan, *The Astrophysical Journal* **861**, 10 (2018).
- [107] H. A. Bethe, *Rev. Mod. Phys.* **62**, 801 (1990).
- [108] A. Burrows, *Rev. Mod. Phys.* **85**, 245 (2013), [arXiv:1210.4921 \[astro-ph.SR\]](#).
- [109] S. E. Woosley and A. Heger, *The Astrophysical Journal* **637**, 914 (2006).
- [110] M. Abernathy and others (ET science team), *Einstein gravitational wave Telescope conceptual design study*, *Tech. Rep. ET-0106C-10* (2011).
- [111] D. Lai and S. L. Shapiro, *Astrophys. J.* **442**, 259 (1995).
- [112] J. D. Brown, in *AIP Conf. Proc. 575: Astrophysical Sources for Ground-Based Gravitational Wave Detectors* (2001) p. 234.
- [113] M. Shibata and Y.-I. Sekiguchi, *Phys. Rev. D.* **71**, 024014 (2005).
- [114] M. Rampp, E. Müller, and M. Ruffert, *Astron. Astrophys.* **332**, 969 (1998).
- [115] C. D. Ott, S. Ou, J. E. Tohline, and A. Burrows, *Astrophys. J.* **625**, L119 (2005).
- [116] C. D. Ott, H. Dimmelmeier, A. Marek, H.-T. Janka, I. Hawke, B. Zink, and E. Schnetter, *Phys. Rev. Lett.* **98**, 261101 (2007).
- [117] L. Santamaria and C. D. Ott, *GWs from Accretion Disk Instabilities*, *Tech. Rep. LIGO-T1100093-v2* (LIGO Scientific Collaboration, 2011).
- [118] G. Pietrzyński *et al.*, *Nature* **567**, 200 (2019).
- [119] P. J. Sutton, (2013), [arXiv:1304.0210 \[gr-qc\]](#).
- [120] J. M. Lattimer and M. Prakash, *Astrophys. J.* **550**, 426 (2001).
- [121] K. Kotake, K. Sato, and K. Takahashi, *Reports on Progress in Physics* **69**, 971 (2006).
- [122] H. J. Lamers and E. M. Levesque, in *Understanding Stellar Evolution*, 2514-3433 (IOP Publishing, 2017) pp. 27–1 to 27–12.
- [123] F. Vissani, *J. Phys. G, Nuc. Phys.* **42**, 013001 (2015), [arXiv:1409.4710 \[astro-ph.HE\]](#).
- [124] S. J. Smartt, *Annual Review of Astronomy and Astrophysics* **47**, 63 (2009).
- [125] M. Tanaka *et al.*, *The Astrophysical Journal* **692**, 1131 (2009), [arXiv:0807.1674 \[astro-ph\]](#).
- [126] V. P. Utrobin and N. N. Chugai, *Astronomy & Astro-*

Authors

B. P. Abbott,¹ R. Abbott,¹ T. D. Abbott,² S. Abraham,³ F. Acernese,^{4,5} K. Ackley,⁶ C. Adams,⁷ V. B. Adya,⁸
 C. Affeldt,^{9,10} M. Agathos,^{11,12} K. Agatsuma,¹³ N. Aggarwal,¹⁴ O. D. Aguiar,¹⁵ L. Aiello,^{16,17} A. Ain,³
 P. Ajith,¹⁸ G. Allen,¹⁹ A. Allocca,^{20,21} M. A. Aloy,²² P. A. Altin,⁸ A. Amato,²³ S. Anand,¹ A. Ananyeva,¹
 S. B. Anderson,¹ W. G. Anderson,²⁴ S. V. Angelova,²⁵ S. Antier,²⁶ S. Appert,¹ K. Arai,¹ M. C. Araya,¹
 J. S. Areeda,²⁷ M. Arène,²⁶ N. Arnaud,^{28,29} S. M. Aronson,³⁰ S. Ascenzi,^{16,31} G. Ashton,⁶ S. M. Aston,⁷
 P. Astone,³² F. Aubin,³³ P. Aufmuth,¹⁰ K. AultONeal,³⁴ C. Austin,² V. Avendano,³⁵ A. Avila-Alvarez,²⁷
 S. Babak,²⁶ P. Bacon,²⁶ F. Badaracco,^{16,17} M. K. M. Bader,³⁶ S. Bae,³⁷ J. Baird,²⁶ P. T. Baker,³⁸
 F. Baldaccini,^{39,40} G. Ballardini,²⁹ S. W. Ballmer,⁴¹ A. Bals,³⁴ S. Banagiri,⁴² J. C. Barayoga,¹ C. Barbieri,^{43,44}
 S. E. Barclay,⁴⁵ B. C. Barish,¹ D. Barker,⁴⁶ K. Barkett,⁴⁷ S. Barnum,¹⁴ F. Barone,^{48,5} B. Barr,⁴⁵ L. Barsotti,¹⁴
 M. Barsuglia,²⁶ D. Barta,⁴⁹ J. Bartlett,⁴⁶ I. Bartos,³⁰ R. Bassiri,⁵⁰ A. Basti,^{20,21} M. Bawaj,^{51,40} J. C. Bayley,⁴⁵
 M. Bazzan,^{52,53} B. Bécsy,⁵⁴ M. Bejger,^{26,55} I. Belahcene,²⁸ A. S. Bell,⁴⁵ D. Beniwal,⁵⁶ M. G. Benjamin,³⁴
 G. Bergmann,^{9,10} S. Bernuzzi,¹¹ C. P. L. Berry,⁵⁷ D. Bersanetti,⁵⁸ A. Bertolini,³⁶ J. Betzwieser,⁷ R. Bhandare,⁵⁹
 J. Bidler,²⁷ E. Biggs,²⁴ I. A. Bilenko,⁶⁰ S. A. Bilgili,³⁸ G. Billingsley,¹ R. Birney,²⁵ O. Birnholtz,⁶¹ S. Biscans,^{1,14}
 M. Bisch,^{62,63} S. Biscoveanu,¹⁴ A. Bisht,¹⁰ M. Bitossi,^{29,21} M. A. Bizouard,⁶⁴ J. K. Blackburn,¹ J. Blackman,⁴⁷
 C. D. Blair,⁷ D. G. Blair,⁶⁵ R. M. Blair,⁴⁶ S. Bloemen,⁶⁶ F. Bobba,^{67,68} N. Bode,^{9,10} M. Boer,⁶⁴ Y. Boetzel,⁶⁹
 G. Bogaert,⁶⁴ F. Bondu,⁷⁰ R. Bonnand,³³ P. Booker,^{9,10} B. A. Boom,³⁶ R. Bork,¹ V. Boschi,²⁹ S. Bose,³
 V. Bossilkov,⁶⁵ J. Bosveld,⁶⁵ Y. Bouffanais,^{52,53} A. Bozzi,²⁹ C. Bradaschia,²¹ P. R. Brady,²⁴ A. Bramley,⁷
 M. Branchesi,^{16,17} J. E. Brau,⁷¹ M. Breschi,¹¹ T. Briant,⁷² J. H. Briggs,⁴⁵ F. Brighenti,^{62,63} A. Brillet,⁶⁴
 M. Brinkmann,^{9,10} P. Brockill,²⁴ A. F. Brooks,¹ J. Brooks,²⁹ D. D. Brown,⁵⁶ S. Brunett,¹ A. Buikema,¹⁴
 T. Bulik,⁷³ H. J. Bulten,^{74,36} A. Buonanno,^{75,76} D. Buskulic,³³ C. Buy,²⁶ R. L. Byer,⁵⁰ M. Cabero,^{9,10}
 L. Cadonati,⁷⁷ G. Cagnoli,⁷⁸ C. Cahillane,¹ J. Calderón Bustillo,⁶ T. A. Callister,¹ E. Calloni,^{79,5} J. B. Camp,⁸⁰
 W. A. Campbell,⁶ M. Canepa,^{81,58} K. C. Cannon,⁸² H. Cao,⁵⁶ J. Cao,⁸³ G. Carapella,^{67,68} F. Carbognani,²⁹
 S. Caride,⁸⁴ M. F. Carney,⁵⁷ G. Carullo,^{20,21} J. Casanueva Diaz,²¹ C. Casentini,^{85,31} S. Caudill,³⁶ M. Cavaglià,^{86,87}
 F. Cavalier,²⁸ R. Cavalieri,²⁹ G. Cella,²¹ P. Cerdá-Durán,²² E. Cesarini,^{88,31} O. Chaibi,⁶⁴ K. Chakravarti,³
 S. J. Chamberlin,⁸⁹ M. Chan,⁴⁵ S. Chao,⁹⁰ P. Charlton,⁹¹ E. A. Chase,⁵⁷ E. Chassande-Mottin,²⁶ D. Chatterjee,²⁴
 M. Chaturvedi,⁵⁹ B. D. Cheeseboro,³⁸ H. Y. Chen,⁹² X. Chen,⁶⁵ Y. Chen,⁴⁷ H.-P. Cheng,³⁰ C. K. Cheong,⁹³
 H. Y. Chia,³⁰ F. Chiadini,^{94,68} A. Chincarini,⁵⁸ A. Chiummo,²⁹ G. Cho,⁹⁵ H. S. Cho,⁹⁶ M. Cho,⁷⁶
 N. Christensen,^{97,64} Q. Chu,⁶⁵ S. Chua,⁷² K. W. Chung,⁹³ S. Chung,⁶⁵ G. Ciani,^{52,53} M. Cieřlar,⁵⁵ A. A. Ciobanu,⁹⁶
 R. Ciolfi,^{98,53} F. Cipriano,⁶⁴ A. Cirone,^{81,58} F. Clara,⁴⁶ J. A. Clark,⁷⁷ P. Clearwater,⁹⁹ F. Cleva,⁶⁴ E. Coccia,^{16,17}
 P.-F. Cohadon,⁷² D. Cohen,²⁸ M. Colleoni,¹⁰⁰ C. G. Collette,¹⁰¹ C. Collins,¹³ M. Colpi,^{43,44} L. R. Cominsky,¹⁰²
 M. Constancio Jr.,¹⁵ L. Conti,⁵³ S. J. Cooper,¹³ P. Corban,⁷ T. R. Corbitt,² I. Cordero-Carrión,¹⁰³ S. Corezzi,^{39,40}
 K. R. Corley,¹⁰⁴ N. Cornish,⁵⁴ D. Corre,²⁸ A. Corsi,⁸⁴ S. Cortese,²⁹ C. A. Costa,¹⁵ R. Cotesta,⁷⁵ M. W. Coughlin,¹
 S. B. Coughlin,^{105,57} J.-P. Coulon,⁶⁴ S. T. Countryman,¹⁰⁴ P. Couvares,¹ P. B. Covas,¹⁰⁰ E. E. Cowan,⁷⁷
 D. M. Coward,⁶⁵ M. J. Cowart,⁷ D. C. Coyne,¹ R. Coyne,¹⁰⁶ J. D. E. Creighton,²⁴ T. D. Creighton,¹⁰⁷ J. Cripe,²
 M. Croquette,⁷² S. G. Crowder,¹⁰⁸ T. J. Cullen,² A. Cumming,⁴⁵ L. Cunningham,⁴⁵ E. Cuoco,²⁹ T. Dal Canton,⁸⁰
 G. Dálya,¹⁰⁹ B. D'Angelo,^{81,58} S. L. Danilishin,^{9,10} S. D'Antonio,³¹ K. Danzmann,^{10,9} A. Dasgupta,¹¹⁰
 C. F. Da Silva Costa,³⁰ L. E. H. Datrier,⁴⁵ V. Dattilo,²⁹ I. Dave,⁵⁹ M. Davier,²⁸ D. Davis,⁴¹ E. J. Daw,¹¹¹
 D. DeBra,⁵⁰ M. Deenadayalan,³ J. Degallaix,²³ M. De Laurentis,^{79,5} S. Deléglise,⁷² W. Del Pozzo,^{20,21}
 L. M. DeMarchi,⁵⁷ N. Demos,¹⁴ T. Dent,¹¹² R. De Pietri,^{113,114} R. De Rosa,^{79,5} C. De Rossi,^{23,29} R. DeSalvo,¹¹⁵
 O. de Varona,^{9,10} S. Dhurandhar,³ M. C. Díaz,¹⁰⁷ T. Dietrich,³⁶ L. Di Fiore,⁵ C. Di Fronzo,¹³ C. Di Giorgio,^{67,68}
 F. Di Giovanni,²² M. Di Giovanni,^{116,117} T. Di Girolamo,^{79,5} A. Di Lieto,^{20,21} B. Ding,¹⁰¹ S. Di Pace,^{118,32}
 I. Di Palma,^{118,32} F. Di Renzo,^{20,21} A. K. Divakarla,³⁰ A. Dmitriev,¹³ Z. Doctor,⁹² F. Donovan,¹⁴
 K. L. Dooley,^{105,86} S. Doravari,³ I. Dorrington,¹⁰⁵ T. P. Downes,²⁴ M. Drago,^{16,17} J. C. Driggers,⁴⁶ Z. Du,⁸³
 J.-G. Ducoin,²⁸ P. Dupej,⁴⁵ O. Durante,^{67,68} S. E. Dwyer,⁴⁶ P. J. Easter,⁶ G. Eddolls,⁴⁵ T. B. Edo,¹¹¹ A. Effler,⁷
 P. Ehrens,¹ J. Eichholz,⁸ S. S. Eikenberry,³⁰ M. Eisenmann,³³ R. A. Eisenstein,¹⁴ L. Errico,^{79,5} R. C. Essick,⁹²
 H. Estelles,¹⁰⁰ D. Estevez,³³ Z. B. Etienne,³⁸ T. Etzel,¹ M. Evans,¹⁴ T. M. Evans,⁷ V. Fafone,^{85,31,16} S. Fairhurst,¹⁰⁵
 X. Fan,⁸³ S. Farinon,⁵⁸ B. Farr,⁷¹ W. M. Farr,¹³ E. J. Fauchon-Jones,¹⁰⁵ M. Favata,³⁵ M. Fays,¹¹¹ M. Fazio,¹¹⁹
 C. Fee,¹²⁰ J. Feicht,¹ M. M. Fejer,⁵⁰ F. Feng,²⁶ A. Fernandez-Galiana,¹⁴ I. Ferrante,^{20,21} E. C. Ferreira,¹⁵
 T. A. Ferreira,¹⁵ F. Fidecaro,^{20,21} I. Fiori,²⁹ D. Fiorucci,^{16,17} M. Fishbach,⁹² R. P. Fisher,¹²¹ J. M. Fishner,¹⁴

- R. Fittipaldi,^{122,68} M. Fitz-Axen,⁴² V. Fiumara,^{123,68} R. Flaminio,^{33,124} M. Fletcher,⁴⁵ E. Floden,⁴² E. Flynn,²⁷ H. Fong,⁸² J. A. Font,^{22,125} P. W. F. Forsyth,⁸ J.-D. Fournier,⁶⁴ Francisco Hernandez Vivanco,⁶ S. Frasca,^{118,32} F. Frasconi,²¹ Z. Frei,¹⁰⁹ A. Freise,¹³ R. Frey,⁷¹ V. Frey,²⁸ P. Fritschel,¹⁴ V. V. Frolov,⁷ G. Fronzè,¹²⁶ P. Fulda,³⁰ M. Fyffe,⁷ H. A. Gabbard,⁴⁵ B. U. Gadre,⁷⁵ S. M. Gaebel,¹³ J. R. Gair,¹²⁷ L. Gammaitoni,³⁹ S. G. Gaonkar,³ C. García-Quirós,¹⁰⁰ F. Garufi,^{79,5} B. Gateley,⁴⁶ S. Gaudio,³⁴ G. Gaur,¹²⁸ V. Gayathri,¹²⁹ G. Gemme,⁵⁸ E. Genin,²⁹ A. Gennai,²¹ D. George,¹⁹ J. George,⁵⁹ L. Gergely,¹³⁰ S. Ghonge,⁷⁷ Abhirup Ghosh,⁷⁵ Archisman Ghosh,³⁶ S. Ghosh,²⁴ B. Giacomazzo,^{116,117} J. A. Giaime,^{2,7} K. D. Giardino,⁷ D. R. Gibson,¹³¹ K. Gill,¹⁰⁴ L. Glover,¹³² J. Griesmer,¹³³ P. Godwin,⁸⁹ E. Goetz,⁴⁶ R. Goetz,³⁰ B. Goncharov,⁶ G. González,² J. M. Gonzalez Castro,^{20,21} A. Gopakumar,¹³⁴ S. E. Gossan,¹ M. Gosselin,^{29,20,21} R. Gouaty,³³ B. Grace,⁸ A. Grado,^{135,5} M. Granata,²³ A. Grant,⁴⁵ S. Gras,¹⁴ P. Grassia,¹ C. Gray,⁴⁶ R. Gray,⁴⁵ G. Greco,^{62,63} A. C. Green,³⁰ R. Green,¹⁰⁵ E. M. Gretarsson,³⁴ A. Grimaldi,^{116,117} S. J. Grimm,^{16,17} P. Groot,⁶⁶ H. Grote,¹⁰⁵ S. Grunewald,⁷⁵ P. Gruning,²⁸ G. M. Guidi,^{62,63} H. K. Gulati,¹¹⁰ Y. Guo,³⁶ A. Gupta,⁸⁹ Anchal Gupta,¹ P. Gupta,³⁶ E. K. Gustafson,¹ R. Gustafson,¹³⁶ L. Haegel,¹⁰⁰ O. Halim,^{17,16} B. R. Hall,¹³⁷ E. D. Hall,¹⁴ E. Z. Hamilton,¹⁰⁵ G. Hammond,⁴⁵ M. Haney,⁶⁹ M. M. Hanke,^{9,10} J. Hanks,⁴⁶ C. Hanna,⁸⁹ M. D. Hannam,¹⁰⁵ O. A. Hannuksela,⁹³ T. J. Hansen,³⁴ J. Hanson,⁷ T. Harder,⁶⁴ T. Hardwick,² K. Haris,¹⁸ J. Harms,^{16,17} G. M. Harry,¹³⁸ I. W. Harry,¹³⁹ R. K. Hasskew,⁷ C. J. Haster,¹⁴ K. Haughian,⁴⁵ F. J. Hayes,⁴⁵ J. Healy,⁶¹ A. Heidmann,⁷² M. C. Heintze,⁷ H. Heitmann,⁶⁴ F. Hellman,¹⁴⁰ P. Hello,²⁸ G. Hemming,²⁹ M. Hendry,⁴⁵ I. S. Heng,⁴⁵ J. Hennig,^{9,10} M. Heurs,^{9,10} S. Hild,⁴⁵ T. Hinderer,^{141,36,142} S. Hochheim,^{9,10} D. Hofman,²³ A. M. Holgado,¹⁹ N. A. Holland,⁸ K. Holt,⁷ D. E. Holz,⁹² P. Hopkins,¹⁰⁵ C. Horst,²⁴ J. Hough,⁴⁵ E. J. Howell,⁶⁵ C. G. Hoy,¹⁰⁵ Y. Huang,¹⁴ M. T. Hübner,⁶ E. A. Huerta,¹⁹ D. Huet,²⁸ B. Hughey,³⁴ V. Hui,³³ S. Husa,¹⁰⁰ S. H. Huttner,⁴⁵ T. Huynh-Dinh,⁷ B. Idzkowski,⁷³ A. Iess,^{85,31} H. Inchauspe,³⁰ C. Ingram,⁵⁶ R. Inta,⁸⁴ G. Intini,^{118,32} B. Irwin,¹²⁰ H. N. Isa,⁴⁵ J.-M. Isac,⁷² M. Isi,¹⁴ B. R. Iyer,¹⁸ T. Jacqmin,⁷² S. J. Jadhav,¹⁴³ K. Jani,⁷⁷ N. N. Jantahalur,¹⁴³ P. Jaranowski,¹⁴⁴ D. Jariwala,³⁰ A. C. Jenkins,¹⁴⁵ J. Jiang,³⁰ D. S. Johnson,¹⁹ A. W. Jones,¹³ D. I. Jones,¹⁴⁶ J. D. Jones,⁴⁶ R. Jones,⁴⁵ R. J. G. Jonker,³⁶ L. Ju,⁶⁵ J. Junker,^{9,10} C. V. Kalaghatgi,¹⁰⁵ V. Kalogera,⁵⁷ B. Kamai,¹ S. Kandhasamy,³ G. Kang,³⁷ J. B. Kanner,¹ S. J. Kapadia,²⁴ S. Karki,⁷¹ R. Kashyap,¹⁸ M. Kasprzak,¹ S. Katsanevas,²⁹ E. Katsavounidis,¹⁴ W. Katzman,⁷ S. Kaufer,¹⁰ K. Kawabe,⁴⁶ N. V. Keerthana,³ F. Kéfélian,⁶⁴ D. Keitel,¹³⁹ R. Kennedy,¹¹¹ J. S. Key,¹⁴⁷ F. Y. Khalili,⁶⁰ I. Khan,^{16,31} S. Khan,^{9,10} E. A. Khazanov,¹⁴⁸ N. Khetan,^{16,17} M. Khurshed,⁵⁹ N. Kijbunchoo,⁸ Chunglee Kim,¹⁴⁹ J. C. Kim,¹⁵⁰ K. Kim,⁹³ W. Kim,⁵⁶ W. S. Kim,¹⁵¹ Y.-M. Kim,¹⁵² C. Kimball,⁵⁷ P. J. King,⁴⁶ M. Kinley-Hanlon,⁴⁵ R. Kirchhoff,^{9,10} J. S. Kissel,⁴⁶ L. Kleybolte,¹³³ J. H. Klika,²⁴ S. Klimentko,³⁰ T. D. Knowles,³⁸ P. Koch,^{9,10} S. M. Koehlenbeck,^{9,10} G. Koekoek,^{36,153} S. Koley,³⁶ V. Kondrashov,¹ A. Kontos,¹⁵⁴ N. Koper,^{9,10} M. Korobko,¹³³ W. Z. Korth,¹ M. Kovalam,⁶⁵ D. B. Kozak,¹ C. Krämer,^{9,10} V. Kringel,^{9,10} N. Krishnendu,¹⁵⁵ A. Królak,^{156,157} N. Krupinski,²⁴ G. Kuehn,^{9,10} A. Kumar,¹⁴³ P. Kumar,¹⁵⁸ Rahul Kumar,⁴⁶ Rakesh Kumar,¹¹⁰ L. Kuo,⁹⁰ A. Kutynia,¹⁵⁶ S. Kwang,²⁴ B. D. Lackey,⁷⁵ D. Laghi,^{20,21} K. H. Lai,⁹³ T. L. Lam,⁹³ M. Landry,⁴⁶ B. B. Lane,¹⁴ R. N. Lang,¹⁵⁹ J. Lange,⁶¹ B. Lantz,⁵⁰ R. K. Lanza,¹⁴ A. Lartaux-Vollard,²⁸ P. D. Lasky,⁶ M. Laxen,⁷ A. Lazzarini,¹ C. Lazzaro,⁵³ P. Leaci,^{118,32} S. Leavey,^{9,10} Y. K. Lecoeuche,⁴⁶ C. H. Lee,⁹⁶ H. K. Lee,¹⁶⁰ H. M. Lee,¹⁶¹ H. W. Lee,¹⁵⁰ J. Lee,⁹⁵ K. Lee,⁴⁵ J. Lehmann,^{9,10} A. K. Lenon,³⁸ N. Leroy,²⁸ N. Letendre,³³ Y. Levin,⁶ A. Li,⁹³ J. Li,⁸³ K. J. L. Li,⁹³ T. G. F. Li,⁹³ X. Li,⁴⁷ F. Lin,⁶ F. Linde,^{162,36} S. D. Linker,¹³² T. B. Littenberg,¹⁶³ J. Liu,⁶⁵ X. Liu,²⁴ M. Llorens-Monteagudo,²² R. K. L. Lo,^{93,1} L. T. London,¹⁴ A. Longo,^{164,165} M. Lorenzini,^{16,17} V. Lorette,¹⁶⁶ M. Lormand,⁷ G. Losurdo,²¹ J. D. Lough,^{9,10} C. O. Lousto,⁶¹ G. Lovelace,²⁷ M. E. Lower,¹⁶⁷ H. Lück,^{10,9} D. Lumaca,^{85,31} A. P. Lundgren,¹³⁹ R. Lynch,¹⁴ Y. Ma,⁴⁷ R. Macas,¹⁰⁵ S. Macfoy,²⁵ M. MacInnis,¹⁴ D. M. Macleod,¹⁰⁵ A. Macquet,⁶⁴ I. Magaña Hernandez,²⁴ F. Magaña-Sandoval,³⁰ R. M. Magee,⁸⁹ E. Majorana,³² I. Maksimovic,¹⁶⁶ A. Malik,⁵⁹ N. Man,⁶⁴ V. Mandic,⁴² V. Mangano,^{45,118,32} G. L. Mansell,^{46,14} M. Manske,²⁴ M. Mantovani,²⁹ M. Mapelli,^{52,53} F. Marchesoni,^{51,40} F. Marion,³³ S. Márka,¹⁰⁴ Z. Márka,¹⁰⁴ C. Markakis,¹⁹ A. S. Markosyan,⁵⁰ A. Markowitz,¹ E. Maros,¹ A. Marquina,¹⁰³ S. Marsat,²⁶ F. Martelli,^{62,63} I. W. Martin,⁴⁵ R. M. Martin,³⁵ V. Martinez,⁷⁸ D. V. Martynov,¹³ H. Masalehdan,¹³³ K. Mason,¹⁴ E. Massera,¹¹¹ A. Masserot,³³ T. J. Massinger,¹ M. Masso-Reid,⁴⁵ S. Mastrogiovanni,²⁶ A. Matas,⁷⁵ F. Matichard,^{1,14} L. Matone,¹⁰⁴ N. Mavalvala,¹⁴ J. J. McCann,⁶⁵ R. McCarthy,⁴⁶ D. E. McClelland,⁸ S. McCormick,⁷ L. McCuller,¹⁴ S. C. McGuire,¹⁶⁸ C. McIsaac,¹³⁹ J. McIver,¹ D. J. McManus,⁸ T. McRae,⁸ S. T. McWilliams,³⁸ D. Meacher,²⁴ G. D. Meadors,⁶ M. Mehmet,^{9,10} A. K. Mehta,¹⁸ J. Meidam,³⁶ E. Mejuto Villa,^{115,68} A. Melatos,⁹⁹ G. Mendell,⁴⁶ R. A. Mercer,²⁴ L. Mereni,²³ K. Merfeld,⁷¹ E. L. Merilh,⁴⁶ M. Merzougui,⁶⁴ S. Meshkov,¹ C. Messenger,⁴⁵ C. Messick,⁸⁹ F. Messina,^{43,44} R. Metzdrorf,⁷² P. M. Meyers,⁹⁹ F. Meylahn,^{9,10} A. Miani,^{116,117} H. Miao,¹³ C. Michel,²³ H. Middleton,⁹⁹ L. Milano,^{79,5} A. L. Miller,^{30,118,32} M. Millhouse,⁹⁹ J. C. Mills,¹⁰⁵ M. C. Milovich-Goff,¹³² O. Minazzoli,^{64,169} Y. Minenkov,³¹ A. Mishkin,³⁰ C. Mishra,¹⁷⁰ T. Mistry,¹¹¹ S. Mitra,³

- V. P. Mitrofanov,⁶⁰ G. Mitselmakher,³⁰ R. Mittleman,¹⁴ G. Mo,⁹⁷ D. Moffa,¹²⁰ K. Mogushi,⁸⁶ S. R. P. Mohapatra,¹⁴ M. Molina-Ruiz,¹⁴⁰ M. Mondin,¹³² M. Montani,^{62,63} C. J. Moore,¹³ D. Moraru,⁴⁶ F. Morawski,⁵⁵ G. Moreno,⁴⁶ S. Morisaki,⁸² B. Mours,³³ C. M. Mow-Lowry,¹³ F. Muciaccia,^{118,32} Arunava Mukherjee,^{9,10} D. Mukherjee,²⁴ S. Mukherjee,¹⁰⁷ Subroto Mukherjee,¹¹⁰ N. Mukund,^{9,10,3} A. Mullavey,⁷ J. Munch,⁵⁶ E. A. Muñiz,⁴¹ M. Muratore,³⁴ P. G. Murray,⁴⁵ I. Nardecchia,^{85,31} L. Naticchioni,^{118,32} R. K. Nayak,¹⁷¹ B. F. Neil,⁶⁵ J. Neilson,^{115,68} G. Nelemans,^{66,36} T. J. N. Nelson,⁷ M. Nery,^{9,10} A. Neunzert,¹³⁶ L. Nevin,¹ K. Y. Ng,¹⁴ S. Ng,⁵⁶ C. Nguyen,²⁶ P. Nguyen,⁷¹ D. Nichols,^{141,36} S. A. Nichols,² S. Nissanke,^{141,36} F. Nocera,²⁹ C. North,¹⁰⁵ L. K. Nuttall,¹³⁹ M. Obergaulinger,^{22,172} J. Oberling,⁴⁶ B. D. O'Brien,³⁰ G. Oganessian,^{16,17} G. H. Ogini,¹⁷³ J. J. Oh,¹⁵¹ S. H. Oh,¹⁵¹ F. Ohme,^{9,10} H. Ohta,⁸² M. A. Okada,¹⁵ M. Oliver,¹⁰⁰ P. Oppermann,^{9,10} Richard J. Oram,⁷ B. O'Reilly,⁷ R. G. Ormiston,⁴² L. F. Ortega,³⁰ R. O'Shaughnessy,⁶¹ S. Ossokine,⁷⁵ D. J. Ottaway,⁵⁶ H. Overmier,⁷ B. J. Owen,⁸⁴ A. E. Pace,⁸⁹ G. Pagano,^{20,21} M. A. Page,⁶⁵ G. Pagliaroli,^{16,17} A. Pai,¹²⁹ S. A. Pai,⁵⁹ J. R. Palamos,⁷¹ O. Palashov,¹⁴⁸ C. Palomba,³² H. Pan,⁹⁰ P. K. Panda,¹⁴³ P. T. H. Pang,^{93,36} C. Pankow,⁵⁷ F. Pannarale,^{118,32} B. C. Pant,⁵⁹ F. Paoletti,²¹ A. Paoli,²⁹ A. Parida,³ W. Parker,^{7,168} D. Pascucci,^{45,36} A. Pasqualetti,²⁹ R. Passaquieti,^{20,21} D. Passuello,²¹ M. Patil,¹⁵⁷ B. Patricelli,^{20,21} E. Payne,⁶ B. L. Pearlstone,⁴⁵ T. C. Pechsiri,³⁰ A. J. Pedersen,⁴¹ M. Pedraza,¹ R. Pedurand,^{23,174} A. Pele,⁷ S. Penn,¹⁷⁵ A. Perego,^{116,117} C. J. Perez,⁴⁶ C. Périgois,³³ A. Perreca,^{116,117} J. Petermann,¹³³ H. P. Pfeiffer,⁷⁵ M. Phelps,^{9,10} K. S. Phukon,³ O. J. Piccinni,^{118,32} M. Pichot,⁶⁴ F. Piergiovanni,^{62,63} V. Pierro,^{115,68} G. Pillant,²⁹ L. Pinard,²³ I. M. Pinto,^{115,68,88} M. Pirello,⁴⁶ M. Pitkin,⁴⁵ W. Plastino,^{164,165} R. Poggiani,^{20,21} D. Y. T. Pong,⁹³ S. Ponrathnam,³ P. Popolizio,²⁹ E. K. Porter,²⁶ J. Powell,¹⁶⁷ A. K. Prajapati,¹¹⁰ J. Prasad,³ K. Prasai,⁵⁰ R. Prasanna,¹⁴³ G. Pratten,¹⁰⁰ T. Prestegard,²⁴ M. Principe,^{115,88,68} G. A. Prodi,^{116,117} L. Prokhorov,¹³ M. Punturo,⁴⁰ P. Puppo,³² M. Pürerer,⁷⁵ H. Qi,¹⁰⁵ V. Quetschke,¹⁰⁷ P. J. Quinonez,³⁴ F. J. Raab,⁴⁶ G. Raaijmakers,^{141,36} H. Radkins,⁴⁶ N. Radulesco,⁶⁴ P. Raffai,¹⁰⁹ S. Raja,⁵⁹ C. Rajan,⁵⁹ B. Rajbhandari,⁸⁴ M. Rakhmanov,¹⁰⁷ K. E. Ramirez,¹⁰⁷ A. Ramos-Buades,¹⁰⁰ Javed Rana,³ K. Rao,⁵⁷ P. Rapagnani,^{118,32} V. Raymond,¹⁰⁵ M. Razzano,^{20,21} J. Read,²⁷ T. Regimbau,³³ L. Rei,⁵⁸ S. Reid,²⁵ D. H. Reitze,^{1,30} P. Rettigno,^{126,176} F. Ricci,^{118,32} C. J. Richardson,³⁴ J. W. Richardson,¹ P. M. Ricker,¹⁹ G. Riemenschneider,^{176,126} K. Riles,¹³⁶ M. Rizzo,⁵⁷ N. A. Robertson,^{1,45} F. Robinet,²⁸ A. Rocchi,³¹ L. Rolland,³³ J. G. Rollins,¹ V. J. Roma,⁷¹ M. Romanelli,⁷⁰ R. Romano,^{4,5} C. L. Romel,⁴⁶ J. H. Romie,⁷ C. A. Rose,²⁴ D. Rose,²⁷ K. Rose,¹²⁰ D. Rosińska,⁷³ S. G. Rosofsky,¹⁹ M. P. Ross,¹⁷⁷ S. Rowan,⁴⁵ A. Rüdiger,^{9,10,a} P. Ruggi,²⁹ G. Rutins,¹³¹ K. Ryan,⁴⁶ S. Sachdev,⁸⁹ T. Sadecki,⁴⁶ M. Sakellariadou,¹⁴⁵ O. S. Salafia,^{178,43,44} L. Salconi,²⁹ M. Saleem,¹⁵⁵ A. Samajdar,³⁶ L. Sammut,⁶ E. J. Sanchez,¹ L. E. Sanchez,¹ N. Sanchis-Gual,¹⁷⁹ J. R. Sanders,¹⁸⁰ K. A. Santiago,³⁵ E. Santos,⁶⁴ N. Sarin,⁶ B. Sassolas,²³ O. Sauter,^{136,33} R. L. Savage,⁴⁶ P. Schale,⁷¹ M. Scheel,⁴⁷ J. Scheuer,⁵⁷ P. Schmidt,^{13,66} R. Schnabel,¹³³ R. M. S. Schofield,⁷¹ A. Schönbeck,¹³³ E. Schreiber,^{9,10} B. W. Schulte,^{9,10} B. F. Schutz,¹⁰⁵ J. Scott,⁴⁵ S. M. Scott,⁸ E. Seidel,¹⁹ D. Sellers,⁷ A. S. Sengupta,¹⁸¹ N. Sennett,⁷⁵ D. Sentenac,²⁹ V. Sequino,⁵⁸ A. Sergeev,¹⁴⁸ Y. Setyawati,^{9,10} D. A. Shaddock,⁸ T. Shaffer,⁴⁶ M. S. Shahriar,⁵⁷ M. B. Shaner,¹³² A. Sharma,^{16,17} P. Sharma,⁵⁹ P. Shawhan,⁷⁶ H. Shen,¹⁹ R. Shink,¹⁸² D. H. Shoemaker,¹⁴ D. M. Shoemaker,⁷⁷ K. Shukla,¹⁴⁰ S. ShyamSundar,⁵⁹ K. Siellez,⁷⁷ M. Sieniawska,⁵⁵ D. Sigg,⁴⁶ L. P. Singer,⁸⁰ D. Singh,⁸⁹ N. Singh,⁷³ A. Singhal,^{16,32} A. M. Sintès,¹⁰⁰ S. Sitmukhambetov,¹⁰⁷ V. Skliris,¹⁰⁵ B. J. J. Slagmolen,⁸ T. J. Slaven-Blair,⁶⁵ J. R. Smith,²⁷ R. J. E. Smith,⁶ S. Somala,¹⁸³ E. J. Son,¹⁵¹ S. Soni,² B. Sorazu,⁴⁵ F. Sorrentino,⁵⁸ T. Souradeep,³ E. Sowell,⁸⁴ A. P. Spencer,⁴⁵ M. Spera,^{52,53} A. K. Srivastava,¹¹⁰ V. Srivastava,⁴¹ K. Staats,⁵⁷ C. Stachie,⁶⁴ M. Standke,^{9,10} D. A. Steer,²⁶ M. Steinke,^{9,10} J. Steinlechner,^{133,45} S. Steinlechner,¹³³ D. Steinmeyer,^{9,10} S. P. Stevenson,¹⁶⁷ D. Stocks,⁵⁰ R. Stone,¹⁰⁷ D. J. Stops,¹³ K. A. Strain,⁴⁵ G. Stratta,^{184,63} S. E. Strigin,⁶⁰ A. Strunk,⁴⁶ R. Sturani,¹⁸⁵ A. L. Stuver,¹⁸⁶ V. Sudhir,¹⁴ T. Z. Summerscales,¹⁸⁷ L. Sun,¹ S. Sunil,¹¹⁰ A. Sur,⁵⁵ J. Suresh,⁸² P. J. Sutton,¹⁰⁵ B. L. Swinkels,³⁶ M. J. Szczepańczyk,³⁴ M. Tacca,³⁶ S. C. Tait,⁴⁵ C. Talbot,⁶ D. B. Tanner,³⁰ D. Tao,¹ M. Tápai,¹³⁰ A. Tapia,²⁷ J. D. Tasson,⁹⁷ R. Taylor,¹ R. Tenorio,¹⁰⁰ L. Terkowski,¹³³ M. Thomas,⁷ P. Thomas,⁴⁶ S. R. Thondapu,⁵⁹ K. A. Thorne,⁷ E. Thrane,⁶ Shubhanshu Tiwari,^{116,117} Srishti Tiwari,¹³⁴ V. Tiwari,¹⁰⁵ K. Toland,⁴⁵ M. Tonelli,^{20,21} Z. Tornasi,⁴⁵ A. Torres-Forné,¹⁸⁸ C. I. Torrie,¹ D. Töyrä,¹³ F. Travasso,^{29,40} G. Traylor,⁷ M. C. Tringali,⁷³ A. Tripathi,¹³⁶ A. Trovato,²⁶ L. Trozzo,^{189,21} K. W. Tsang,³⁶ M. Tse,¹⁴ R. Tso,⁴⁷ L. Tsukada,⁸² D. Tsuna,⁸² T. Tsutsui,⁸² D. Tuyenbayev,¹⁰⁷ K. Ueno,⁸² D. Ugolini,¹⁹⁰ C. S. Unnikrishnan,¹³⁴ A. L. Urban,² S. A. Usman,⁹² H. Vahlbruch,¹⁰ G. Vajente,¹ G. Valdes,² M. Valentini,^{116,117} N. van Bakel,³⁶ M. van Beuzekom,³⁶ J. F. J. van den Brand,^{74,36} C. Van Den Broeck,^{36,191} D. C. Vander-Hyde,⁴¹ L. van der Schaaf,³⁶ J. V. VanHeijningen,⁶⁵ A. A. van Veggel,⁴⁵ M. Vardaro,^{52,53} V. Varma,⁴⁷ S. Vass,¹ M. Vasúth,⁴⁹ A. Vecchio,¹³ G. Vedovato,⁵³ J. Veitch,⁴⁵ P. J. Veitch,⁵⁶ K. Venkateswara,¹⁷⁷ G. Venugopalan,¹ D. Verkindt,³³ F. Vetrano,^{62,63} A. Viceré,^{62,63} A. D. Viets,²⁴ S. Vinciguerra,¹³ D. J. Vine,¹³¹ J.-Y. Vinet,⁶⁴ S. Vitale,¹⁴ T. Vo,⁴¹ H. Vocca,^{39,40} C. Vorvick,⁴⁶ S. P. Vyatchanin,⁶⁰ A. R. Wade,¹

L. E. Wade,¹²⁰ M. Wade,¹²⁰ R. Walet,³⁶ M. Walker,²⁷ L. Wallace,¹ S. Walsh,²⁴ H. Wang,¹³ J. Z. Wang,¹³⁶ S. Wang,¹⁹ W. H. Wang,¹⁰⁷ Y. F. Wang,⁹³ R. L. Ward,⁸ Z. A. Warden,³⁴ J. Warner,⁴⁶ M. Was,³³ J. Watchi,¹⁰¹ B. Weaver,⁴⁶ L.-W. Wei,^{9,10} M. Weinert,^{9,10} A. J. Weinstein,¹ R. Weiss,¹⁴ F. Wellmann,^{9,10} L. Wen,⁶⁵ E. K. Wessel,¹⁹ P. Weßels,^{9,10} J. W. Westhouse,³⁴ K. Wette,⁸ J. T. Whelan,⁶¹ B. F. Whiting,³⁰ C. Whittle,¹⁴ D. M. Wilken,^{9,10} D. Williams,⁴⁵ A. R. Williamson,^{141,36} J. L. Willis,¹ B. Willke,^{10,9} W. Winkler,^{9,10} C. C. Wipf,¹ H. Wittel,^{9,10} G. Woan,⁴⁵ J. Woehler,^{9,10} J. K. Wofford,⁶¹ J. L. Wright,⁴⁵ D. S. Wu,^{9,10} D. M. Wysocki,⁶¹ S. Xiao,¹ R. Xu,¹⁰⁸ H. Yamamoto,¹ C. C. Yancey,⁷⁶ L. Yang,¹¹⁹ Y. Yang,³⁰ Z. Yang,⁴² M. J. Yap,⁸ M. Yazback,³⁰ D. W. Yeeles,¹⁰⁵ Hang Yu,¹⁴ Haocun Yu,¹⁴ S. H. R. Yuen,⁹³ A. K. Zdrożny,¹⁰⁷ A. Zdrożny,¹⁵⁶ M. Zanolin,³⁴ T. Zelenova,²⁹ J.-P. Zendri,⁵³ M. Zevin,⁵⁷ J. Zhang,⁶⁵ L. Zhang,¹ T. Zhang,⁴⁵ C. Zhao,⁶⁵ G. Zhao,¹⁰¹ M. Zhou,⁵⁷ Z. Zhou,⁵⁷ X. J. Zhu,⁶ M. E. Zucker,^{1,14} and J. Zweigig¹

(The LIGO Scientific Collaboration and the Virgo Collaboration)

T. W.-S. Holoien,¹⁹² C. S. Kochanek,^{193,194} J. L. Prieto,^{195,196} B. J. Shappee,¹⁹⁷ and K. Z. Stanek^{193,194}

(The ASAS-SN Collaboration)

J. Haislip,¹⁹⁸ V. Kouprianov,^{198,199} D. E. Reichart,¹⁹⁸ D. J. Sand,²⁰⁰ L. Tartaglia,²⁰¹ S. Valenti,²⁰² S. Wyatt,²⁰⁰ and S. Yang^{202,203,204}

(The DLT40 Collaboration)

F. Salemi²⁰⁵

¹*LIGO, California Institute of Technology, Pasadena, CA 91125, USA*

²*Louisiana State University, Baton Rouge, LA 70803, USA*

³*Inter-University Centre for Astronomy and Astrophysics, Pune 411007, India*

⁴*Dipartimento di Farmacia, Università di Salerno, I-84084 Fisciano, Salerno, Italy*

⁵*INFN, Sezione di Napoli, Complesso Universitario di Monte S. Angelo, I-80126 Napoli, Italy*

⁶*OzGrav, School of Physics & Astronomy, Monash University, Clayton 3800, Victoria, Australia*

⁷*LIGO Livingston Observatory, Livingston, LA 70754, USA*

⁸*OzGrav, Australian National University, Canberra, Australian Capital Territory 0200, Australia*

⁹*Max Planck Institute for Gravitational Physics (Albert Einstein Institute), D-30167 Hannover, Germany*

¹⁰*Leibniz Universität Hannover, D-30167 Hannover, Germany*

¹¹*Theoretisch-Physikalisches Institut, Friedrich-Schiller-Universität Jena, D-07743 Jena, Germany*

¹²*University of Cambridge, Cambridge CB2 1TN, United Kingdom*

¹³*University of Birmingham, Birmingham B15 2TT, United Kingdom*

¹⁴*LIGO, Massachusetts Institute of Technology, Cambridge, MA 02139, USA*

¹⁵*Instituto Nacional de Pesquisas Espaciais, 12227-010 São José dos Campos, São Paulo, Brazil*

¹⁶*Gran Sasso Science Institute (GSSI), I-67100 L'Aquila, Italy*

¹⁷*INFN, Laboratori Nazionali del Gran Sasso, I-67100 Assergi, Italy*

¹⁸*International Centre for Theoretical Sciences, Tata Institute of Fundamental Research, Bengaluru 560089, India*

¹⁹*NCSA, University of Illinois at Urbana-Champaign, Urbana, IL 61801, USA*

²⁰*Università di Pisa, I-56127 Pisa, Italy*

²¹*INFN, Sezione di Pisa, I-56127 Pisa, Italy*

²²*Departamento de Astronomía y Astrofísica, Universitat de València, E-46100 Burjassot, València, Spain*

²³*Laboratoire des Matériaux Avancés (LMA), CNRS/IN2P3, F-69622 Villeurbanne, France*

²⁴*University of Wisconsin-Milwaukee, Milwaukee, WI 53201, USA*

²⁵*SUPA, University of Strathclyde, Glasgow G1 1XQ, United Kingdom*

²⁶*APC, AstroParticule et Cosmologie, Université Paris Diderot, CNRS/IN2P3, CEA/Irfu, Observatoire de Paris, Sorbonne Paris Cité, F-75205 Paris Cedex 13, France*

²⁷*California State University Fullerton, Fullerton, CA 92831, USA*

²⁸*LAL, Univ. Paris-Sud, CNRS/IN2P3, Université Paris-Saclay, F-91898 Orsay, France*

²⁹*European Gravitational Observatory (EGO), I-56021 Cascina, Pisa, Italy*

³⁰*University of Florida, Gainesville, FL 32611, USA*

³¹*INFN, Sezione di Roma Tor Vergata, I-00133 Roma, Italy*

³²*INFN, Sezione di Roma, I-00185 Roma, Italy*

³³*Laboratoire d'Annecy de Physique des Particules (LAPP), Univ. Grenoble Alpes, Université Savoie Mont Blanc, CNRS/IN2P3, F-74941 Annecy, France*

³⁴*Embry-Riddle Aeronautical University, Prescott, AZ 86301, USA*

³⁵*Montclair State University, Montclair, NJ 07043, USA*

³⁶*Nikhef, Science Park 105, 1098 XG Amsterdam, The Netherlands*

- ³⁷ *Korea Institute of Science and Technology Information, Daejeon 34141, South Korea*
- ³⁸ *West Virginia University, Morgantown, WV 26506, USA*
- ³⁹ *Università di Perugia, I-06123 Perugia, Italy*
- ⁴⁰ *INFN, Sezione di Perugia, I-06123 Perugia, Italy*
- ⁴¹ *Syracuse University, Syracuse, NY 13244, USA*
- ⁴² *University of Minnesota, Minneapolis, MN 55455, USA*
- ⁴³ *Università degli Studi di Milano-Bicocca, I-20126 Milano, Italy*
- ⁴⁴ *INFN, Sezione di Milano-Bicocca, I-20126 Milano, Italy*
- ⁴⁵ *SUPA, University of Glasgow, Glasgow G12 8QQ, United Kingdom*
- ⁴⁶ *LIGO Hanford Observatory, Richland, WA 99352, USA*
- ⁴⁷ *Caltech CaRT, Pasadena, CA 91125, USA*
- ⁴⁸ *Dipartimento di Medicina, Chirurgia e Odontoiatria “Scuola Medica Salernitana,
” Università di Salerno, I-84081 Baronissi, Salerno, Italy*
- ⁴⁹ *Wigner RCP, RMKI, H-1121 Budapest, Konkoly Thege Miklós út 29-33, Hungary*
- ⁵⁰ *Stanford University, Stanford, CA 94305, USA*
- ⁵¹ *Università di Camerino, Dipartimento di Fisica, I-62032 Camerino, Italy*
- ⁵² *Università di Padova, Dipartimento di Fisica e Astronomia, I-35131 Padova, Italy*
- ⁵³ *INFN, Sezione di Padova, I-35131 Padova, Italy*
- ⁵⁴ *Montana State University, Bozeman, MT 59717, USA*
- ⁵⁵ *Nicolaus Copernicus Astronomical Center, Polish Academy of Sciences, 00-716, Warsaw, Poland*
- ⁵⁶ *OzGrav, University of Adelaide, Adelaide, South Australia 5005, Australia*
- ⁵⁷ *Center for Interdisciplinary Exploration & Research in Astrophysics (CIERA),
Northwestern University, Evanston, IL 60208, USA*
- ⁵⁸ *INFN, Sezione di Genova, I-16146 Genova, Italy*
- ⁵⁹ *RRCAT, Indore, Madhya Pradesh 452013, India*
- ⁶⁰ *Faculty of Physics, Lomonosov Moscow State University, Moscow 119991, Russia*
- ⁶¹ *Rochester Institute of Technology, Rochester, NY 14623, USA*
- ⁶² *Università degli Studi di Urbino “Carlo Bo,” I-61029 Urbino, Italy*
- ⁶³ *INFN, Sezione di Firenze, I-50019 Sesto Fiorentino, Firenze, Italy*
- ⁶⁴ *Artemis, Université Côte d’Azur, Observatoire Côte d’Azur,
CNRS, CS 34229, F-06304 Nice Cedex 4, France*
- ⁶⁵ *OzGrav, University of Western Australia, Crawley, Western Australia 6009, Australia*
- ⁶⁶ *Department of Astrophysics/IMAPP, Radboud University Nijmegen,
P.O. Box 9010, 6500 GL Nijmegen, The Netherlands*
- ⁶⁷ *Dipartimento di Fisica “E.R. Caianiello,” Università di Salerno, I-84084 Fisciano, Salerno, Italy*
- ⁶⁸ *INFN, Sezione di Napoli, Gruppo Collegato di Salerno,
Complesso Universitario di Monte S. Angelo, I-80126 Napoli, Italy*
- ⁶⁹ *Physik-Institut, University of Zurich, Winterthurerstrasse 190, 8057 Zurich, Switzerland*
- ⁷⁰ *Univ Rennes, CNRS, Institut FOTON - UMR6082, F-3500 Rennes, France*
- ⁷¹ *University of Oregon, Eugene, OR 97403, USA*
- ⁷² *Laboratoire Kastler Brossel, Sorbonne Université, CNRS,
ENS-Université PSL, Collège de France, F-75005 Paris, France*
- ⁷³ *Astronomical Observatory Warsaw University, 00-478 Warsaw, Poland*
- ⁷⁴ *VU University Amsterdam, 1081 HV Amsterdam, The Netherlands*
- ⁷⁵ *Max Planck Institute for Gravitational Physics (Albert Einstein Institute), D-14476 Potsdam-Golm, Germany*
- ⁷⁶ *University of Maryland, College Park, MD 20742, USA*
- ⁷⁷ *School of Physics, Georgia Institute of Technology, Atlanta, GA 30332, USA*
- ⁷⁸ *Université de Lyon, Université Claude Bernard Lyon 1,
CNRS, Institut Lumière Matière, F-69622 Villeurbanne, France*
- ⁷⁹ *Università di Napoli “Federico II,” Complesso Universitario di Monte S. Angelo, I-80126 Napoli, Italy*
- ⁸⁰ *NASA Goddard Space Flight Center, Greenbelt, MD 20771, USA*
- ⁸¹ *Dipartimento di Fisica, Università degli Studi di Genova, I-16146 Genova, Italy*
- ⁸² *RESCEU, University of Tokyo, Tokyo, 113-0033, Japan.*
- ⁸³ *Tsinghua University, Beijing 100084, China*
- ⁸⁴ *Texas Tech University, Lubbock, TX 79409, USA*
- ⁸⁵ *Università di Roma Tor Vergata, I-00133 Roma, Italy*
- ⁸⁶ *The University of Mississippi, University, MS 38677, USA*
- ⁸⁷ *Missouri University of Science and Technology, Rolla, MO 65409, USA*
- ⁸⁸ *Museo Storico della Fisica e Centro Studi e Ricerche “Enrico Fermi,” I-00184 Roma, Italy*
- ⁸⁹ *The Pennsylvania State University, University Park, PA 16802, USA*
- ⁹⁰ *National Tsing Hua University, Hsinchu City, 30013 Taiwan, Republic of China*
- ⁹¹ *Charles Sturt University, Wagga Wagga, New South Wales 2678, Australia*
- ⁹² *University of Chicago, Chicago, IL 60637, USA*
- ⁹³ *The Chinese University of Hong Kong, Shatin, NT, Hong Kong*

- ⁹⁴ *Dipartimento di Ingegneria Industriale (DIIN),
Università di Salerno, I-84084 Fisciano, Salerno, Italy*
- ⁹⁵ *Seoul National University, Seoul 08826, South Korea*
- ⁹⁶ *Pusan National University, Busan 46241, South Korea*
- ⁹⁷ *Carleton College, Northfield, MN 55057, USA*
- ⁹⁸ *INAF, Osservatorio Astronomico di Padova, I-35122 Padova, Italy*
- ⁹⁹ *OzGrav, University of Melbourne, Parkville, Victoria 3010, Australia*
- ¹⁰⁰ *Universitat de les Illes Balears, IAC3—IEEC, E-07122 Palma de Mallorca, Spain*
- ¹⁰¹ *Université Libre de Bruxelles, Brussels 1050, Belgium*
- ¹⁰² *Sonoma State University, Rohnert Park, CA 94928, USA*
- ¹⁰³ *Departamento de Matemáticas, Universitat de València, E-46100 Burjassot, València, Spain*
- ¹⁰⁴ *Columbia University, New York, NY 10027, USA*
- ¹⁰⁵ *Cardiff University, Cardiff CF24 3AA, United Kingdom*
- ¹⁰⁶ *University of Rhode Island, Kingston, RI 02881, USA*
- ¹⁰⁷ *The University of Texas Rio Grande Valley, Brownsville, TX 78520, USA*
- ¹⁰⁸ *Bellevue College, Bellevue, WA 98007, USA*
- ¹⁰⁹ *MTA-ELTE Astrophysics Research Group, Institute of Physics, Eötvös University, Budapest 1117, Hungary*
- ¹¹⁰ *Institute for Plasma Research, Bhat, Gandhinagar 382428, India*
- ¹¹¹ *The University of Sheffield, Sheffield S10 2TN, United Kingdom*
- ¹¹² *IGFAE, Campus Sur, Universidade de Santiago de Compostela, 15782 Spain*
- ¹¹³ *Dipartimento di Scienze Matematiche, Fisiche e Informatiche, Università di Parma, I-43124 Parma, Italy*
- ¹¹⁴ *INFN, Sezione di Milano Bicocca, Gruppo Collegato di Parma, I-43124 Parma, Italy*
- ¹¹⁵ *Dipartimento di Ingegneria, Università del Sannio, I-82100 Benevento, Italy*
- ¹¹⁶ *Università di Trento, Dipartimento di Fisica, I-38123 Povo, Trento, Italy*
- ¹¹⁷ *INFN, Trento Institute for Fundamental Physics and Applications, I-38123 Povo, Trento, Italy*
- ¹¹⁸ *Università di Roma “La Sapienza,” I-00185 Roma, Italy*
- ¹¹⁹ *Colorado State University, Fort Collins, CO 80523, USA*
- ¹²⁰ *Kenyon College, Gambier, OH 43022, USA*
- ¹²¹ *Christopher Newport University, Newport News, VA 23606, USA*
- ¹²² *CNR-SPIN, c/o Università di Salerno, I-84084 Fisciano, Salerno, Italy*
- ¹²³ *Scuola di Ingegneria, Università della Basilicata, I-85100 Potenza, Italy*
- ¹²⁴ *National Astronomical Observatory of Japan, 2-21-1 Osawa, Mitaka, Tokyo 181-8588, Japan*
- ¹²⁵ *Observatori Astronòmic, Universitat de València, E-46980 Paterna, València, Spain*
- ¹²⁶ *INFN Sezione di Torino, I-10125 Torino, Italy*
- ¹²⁷ *School of Mathematics, University of Edinburgh, Edinburgh EH9 3FD, United Kingdom*
- ¹²⁸ *Institute Of Advanced Research, Gandhinagar 382426, India*
- ¹²⁹ *Indian Institute of Technology Bombay, Powai, Mumbai 400 076, India*
- ¹³⁰ *University of Szeged, Dóm tér 9, Szeged 6720, Hungary*
- ¹³¹ *SUPA, University of the West of Scotland, Paisley PA1 2BE, United Kingdom*
- ¹³² *California State University, Los Angeles, 5151 State University Dr, Los Angeles, CA 90032, USA*
- ¹³³ *Universität Hamburg, D-22761 Hamburg, Germany*
- ¹³⁴ *Tata Institute of Fundamental Research, Mumbai 400005, India*
- ¹³⁵ *INAF, Osservatorio Astronomico di Capodimonte, I-80131 Napoli, Italy*
- ¹³⁶ *University of Michigan, Ann Arbor, MI 48109, USA*
- ¹³⁷ *Washington State University, Pullman, WA 99164, USA*
- ¹³⁸ *American University, Washington, D.C. 20016, USA*
- ¹³⁹ *University of Portsmouth, Portsmouth, PO1 3FX, United Kingdom*
- ¹⁴⁰ *University of California, Berkeley, CA 94720, USA*
- ¹⁴¹ *GRAPPA, Anton Pannekoek Institute for Astronomy and Institute for High-Energy Physics,
University of Amsterdam, Science Park 904, 1098 XH Amsterdam, The Netherlands*
- ¹⁴² *Delta Institute for Theoretical Physics, Science Park 904, 1090 GL Amsterdam, The Netherlands*
- ¹⁴³ *Directorate of Construction, Services & Estate Management, Mumbai 400094 India*
- ¹⁴⁴ *University of Białystok, 15-424 Białystok, Poland*
- ¹⁴⁵ *King’s College London, University of London, London WC2R 2LS, United Kingdom*
- ¹⁴⁶ *University of Southampton, Southampton SO17 1BJ, United Kingdom*
- ¹⁴⁷ *University of Washington Bothell, Bothell, WA 98011, USA*
- ¹⁴⁸ *Institute of Applied Physics, Nizhny Novgorod, 603950, Russia*
- ¹⁴⁹ *Ewha Womans University, Seoul 03760, South Korea*
- ¹⁵⁰ *Inje University Gimhae, South Gyeongsang 50834, South Korea*
- ¹⁵¹ *National Institute for Mathematical Sciences, Daejeon 34047, South Korea*
- ¹⁵² *Ulsan National Institute of Science and Technology, Ulsan 44919, South Korea*
- ¹⁵³ *Maastricht University, P.O. Box 616, 6200 MD Maastricht, The Netherlands*
- ¹⁵⁴ *Bard College, 30 Campus Rd, Annandale-On-Hudson, NY 12504, USA*
- ¹⁵⁵ *Chennai Mathematical Institute, Chennai 603103, India*

- ¹⁵⁶ NCBJ, 05-400 Świerk-Otwock, Poland
- ¹⁵⁷ Institute of Mathematics, Polish Academy of Sciences, 00656 Warsaw, Poland
- ¹⁵⁸ Cornell University, Ithaca, NY 14850, USA
- ¹⁵⁹ Hillsdale College, Hillsdale, MI 49242, USA
- ¹⁶⁰ Hanyang University, Seoul 04763, South Korea
- ¹⁶¹ Korea Astronomy and Space Science Institute, Daejeon 34055, South Korea
- ¹⁶² Institute for High-Energy Physics, University of Amsterdam,
Science Park 904, 1098 XH Amsterdam, The Netherlands
- ¹⁶³ NASA Marshall Space Flight Center, Huntsville, AL 35811, USA
- ¹⁶⁴ Dipartimento di Matematica e Fisica, Università degli Studi Roma Tre, I-00146 Roma, Italy
- ¹⁶⁵ INFN, Sezione di Roma Tre, I-00146 Roma, Italy
- ¹⁶⁶ ESPCI, CNRS, F-75005 Paris, France
- ¹⁶⁷ OzGrav, Swinburne University of Technology, Hawthorn VIC 3122, Australia
- ¹⁶⁸ Southern University and A&M College, Baton Rouge, LA 70813, USA
- ¹⁶⁹ Centre Scientifique de Monaco, 8 quai Antoine 1er, MC-98000, Monaco
- ¹⁷⁰ Indian Institute of Technology Madras, Chennai 600036, India
- ¹⁷¹ IISER-Kolkata, Mohanpur, West Bengal 741252, India
- ¹⁷² Institut für Kernphysik, Theoriezentrum, 64289 Darmstadt, Germany
- ¹⁷³ Whitman College, 345 Boyer Avenue, Walla Walla, WA 99362 USA
- ¹⁷⁴ Université de Lyon, F-69361 Lyon, France
- ¹⁷⁵ Hobart and William Smith Colleges, Geneva, NY 14456, USA
- ¹⁷⁶ Dipartimento di Fisica, Università degli Studi di Torino, I-10125 Torino, Italy
- ¹⁷⁷ University of Washington, Seattle, WA 98195, USA
- ¹⁷⁸ INAF, Osservatorio Astronomico di Brera sede di Merate, I-23807 Merate, Lecco, Italy
- ¹⁷⁹ Centro de Astrofísica e Gravitação (CENTRA),
Departamento de Física, Instituto Superior Técnico,
Universidade de Lisboa, 1049-001 Lisboa, Portugal
- ¹⁸⁰ Marquette University, 11420 W. Clybourn St., Milwaukee, WI 53233, USA
- ¹⁸¹ Indian Institute of Technology, Gandhinagar Ahmedabad Gujarat 382424, India
- ¹⁸² Université de Montréal/Polytechnique, Montreal, Quebec H3T 1J4, Canada
- ¹⁸³ Indian Institute of Technology Hyderabad, Sangareddy, Khandi, Telangana 502285, India
- ¹⁸⁴ INAF, Osservatorio di Astrofisica e Scienza dello Spazio, I-40129 Bologna, Italy
- ¹⁸⁵ International Institute of Physics, Universidade Federal do Rio Grande do Norte, Natal RN 59078-970, Brazil
- ¹⁸⁶ Villanova University, 800 Lancaster Ave, Villanova, PA 19085, USA
- ¹⁸⁷ Andrews University, Berrien Springs, MI 49104, USA
- ¹⁸⁸ Max Planck Institute for Gravitationalphysik (Albert Einstein Institute), D-14476 Potsdam-Golm, Germany
- ¹⁸⁹ Università di Siena, I-53100 Siena, Italy
- ¹⁹⁰ Trinity University, San Antonio, TX 78212, USA
- ¹⁹¹ Van Swinderen Institute for Particle Physics and Gravity,
University of Groningen, Nijenborgh 4, 9747 AG Groningen, The Netherlands
- ¹⁹² Carnegie Observatories, 813 Santa Barbara Street, Pasadena, CA 91101, USA
- ¹⁹³ Department of Astronomy, The Ohio State University,
140 West 18th Avenue, Columbus, OH 43210, USA
- ¹⁹⁴ Center for Cosmology and AstroParticle Physics, The Ohio State University,
191 W. Woodruff Ave., Columbus, OH 43210, USA
- ¹⁹⁵ Núcleo de Astronomía de la Facultad de Ingeniería,
Universidad Diego Portales, Av. Ejército 441, Santiago, Chile
- ¹⁹⁶ Millennium Institute of Astrophysics, Santiago, Chile
- ¹⁹⁷ Institute for Astronomy, University of Hawai'i,
2680 Woodlawn Drive, Honolulu, HI 96822, USA
- ¹⁹⁸ Department of Physics and Astronomy, University of North Carolina at Chapel Hill, Chapel Hill, NC 27599, USA
- ¹⁹⁹ Central (Pulkovo) Observatory of Russian Academy of Sciences,
196140 Pulkovskoye Ave. 65/1, Saint Petersburg, Russia
- ²⁰⁰ Department of Astronomy/Steward Observatory,
933 North Cherry Avenue, Room N204, Tucson, AZ 85721-0065, USA
- ²⁰¹ Department of Astronomy and The Oskar Klein Centre,
AlbaNova University Center, Stockholm University, SE-106 91 Stockholm, Sweden
- ²⁰² Department of Physics, University of California, 1 Shields Avenue, Davis, CA 95616-5270, USA
- ²⁰³ Department of Physics and Astronomy Galileo Galilei,
University of Padova, Vicolo dell'Osservatorio, 3, I-35122 Padova, Italy
- ²⁰⁴ INAF Osservatorio Astronomico di Padova, Vicolo dell'Osservatorio 5, I-35122 Padova, Italy
- ²⁰⁵ Albert-Einstein-Institut, Max-Planck-Institut für Gravitationsphysik, D-30167 Hannover, Germany

(Dated: 22 August 2019)

PACS numbers: 04.80.Nn, 07.05.Kf, 95.85.Sz, 97.60.Bw

^a Deceased, July 2018.